Ribeiro, F.; Sena-Cruz, J.; Branco, F.G.; Júlio, E. (2018) "Hybrid effect and pseudo-ductile behaviour of unidirectional interlayer hybrid FRP composites for civil engineering applications." Construction & Building Materials, 171:871–890.

Hybrid effect and pseudo-ductile behaviour of unidirectional interlayer hybrid FRP composites for civil engineering applications

Filipe Ribeiro[1], José Sena-Cruz[2]*, Fernando G. Branco[3], Eduardo Júlio[4]

Abstract: An experimental study on the tensile stress–strain curves of interlayer (layer-by-layer) unidirectional hybrid FRP composites was conducted aiming at evaluating the corresponding hybrid effect and pseudo-ductility of this innovative solution. Different combinations of the following dry unidirectional fabric materials, also varying the number of layers, were adopted in tests: high-modulus carbon, standard carbon, E-glass, and basalt. The composites were produced layer-by-layer by hand lay-up method, using an epoxy-based resin as matrix. The results have shown a strain increase at failure of both standard carbon and high-modulus carbon fibres with the volume decrease of these materials in hybrid combinations. It was also concluded that combining high-modulus carbon with E-glass, high-modulus carbon with basalt, or high-modulus carbon with standard carbon can lead to very good pseudo-ductile tensile behaviour. Finally, it should be highlighted that an existing analytical model in the literature was satisfactorily adopted to predict the tensile response of these hybrid composites.

Keywords: Hybrid composite; Fragmentation; Mechanical properties; Analytical modelling

[1] PhD Student, CERIS, Instituto Superior Técnico, Universidade de Lisboa, Portugal. E-mail: filipe.t.ribeiro@tecnico.ulisboa.pt
[2] Associate Professor, ISISE, Department of Civil Engineering, University of Minho, Portugal. E-mail: jsena@civil.uminho.pt *Corresponding Author
[3] Assistant Professor, ISISE, Department of Civil Engineering, University of Coimbra, Portugal. E-mail: fjbranco@dec.uc.pt
[4] Full Professor, CERIS, Instituto Superior Técnico, Universidade de Lisboa, Portugal. E-mail: eduardo.julio@tecnico.ulisboa.pt

1 INTRODUCTION

Unidirectional (UD) Fibre Reinforced Polymers (FRP) composites are brittle materials, exhibiting a linear elastic behaviour up to failure. Therefore, structures made of these materials, although apparently without any problem, may fail abruptly [1]. This characteristic does not allow to take full advantage of FRP properties, namely the high tensile strength due to conservative design limits [2]. For this reason, to obtain composites with progressive failure behaviour ensuring safe, strain hardening, and meaningful ultimate tension strain are seen as priority goal by different industries [2], including civil engineering.

Hybridisation, i.e., the incorporation of two or more types of fibres within the same polymeric matrix [3], is an established approach to deal with the problem above mentioned, since this strategy promotes synergies between the adopted reinforcing materials, lessening their intrinsic disadvantages [4]. For instance, when submitted to uniaxial tension, Low Strain (LS) fibres fail earlier than High Strain (HS) fibres and this fracture behaviour can be used as a warning sign before the ultimate failure of the hybrid FRP composite [1, 4]. Furthermore, it has been observed that hybridisation increases the apparent strain at LS fibres failure [5]. This phenomenon has been described as "hybrid effect" [6]. In the case of carbon/glass hybrid composites, the values for this effect are typically in the range of 10 to 50% [4]. Nowadays, however, there is some controversy about the hybrid effect definition because, in traditional uniaxial tensile testing configuration, stress concentration at the grips may cause premature composite failure, leading to an underestimation of the strain at the failure of the baseline LS material [7]. For this reason, these results should be critically interpreted.

Nevertheless, the most relevant advantage of hybrid composites is their gradual, and thus non-catastrophic, failure mode that has been registered in UD layer-by-layer configurations [2, 8], when both the configuration and materials combination are appropriately selected. This is due to the load transfer between LS and HS layers, fragmentation (a damage process where multiple fractures take place) of the formers, followed by the stable delamination of the LS layers from the HS layers, close to the LS layer fractures, ending with the failure of the latter [1]. This behaviour is known as pseudo-ductility [1, 4]. It should be stressed that the term 'pseudo-ductility' is used because it is possible to achieve a flat-topped stress-strain curve of monotonic tensile tests up to the failure of some unidirectional hybrid FRP composites.

The topic of hybrid composites has become a highly active research area in the 1970's and 1980's [3, 5, 9-16]. Over the time, several literature reviews on this subject were published [3, 4, 16]. The study of hybrid composites was essentially motivated in the scope of the aerospace and automotive industries [3, 4, 17]. It has been demonstrated that hybrid composites have greater advantages over traditional composites. The vast majority

of the works published generally reported mechanical tension test results of hybrid composites indicating: (i) a linear increase of elastic modulus in respect to HS material (generally glass fibres) with the addition of LS material (in most part of cases, carbon fibres) [3], (ii) a load drop at the LS material fracture (in non-catastrophic cases), and (iii) a significant hybrid effect [2].

Swolfs *et al.* [18] explained that, in non-hybrid UD composites, when a fibre fails, it locally loses its load transfer capability. The surrounding matrix is loaded in shear and transfers the load carried out by the broken fibre to the surrounding ones, increasing their probability of break. When enough neighbouring fibres are broken, a critical cluster size is reached and catastrophic failure occurs. The restriction caused by HS fibres adjacent to a LS fibre broken, has been reported as the main factor contributing for the hybrid effect, since HS fibres inhibit the formation of critical clusters [4, 7]. However, other reasons for the hybrid effect have been pointed out, namely: (i) thermal residual stresses, i.e., residual shrinkage stresses due to differences in the thermal contraction of the two fibre types, and (ii) the modification, relatively to non-hybrid composites, of the temporary dynamic stress concentrations, due to stress wave travelling along each fibre when it fails [4]. The latter has received no attention at all in the past two decades and remains poorly investigated today [4].

Recently, Swolfs and his co-authors have carried out extensive work aiming at understanding the hybrid effect [18-25]. In [21], the effect of fibres dispersion on the initial strain at the failure and cluster development in UD carbon/glass hybrid composites was numerically studied. It was concluded that the strain at the failure of carbon fibre composites can be dramatically increased with a large fraction of well-dispersed glass fibres. However, random dispersion configurations are not the best option to achieve maximum hybrid effect. Layer-by-layer hybrids are more efficient in delaying the failure development. Furthermore, it was indicated that the hybrid effect gradually increases with the increase in volume fraction of HS fibres. In [24] and [25], it was demonstrated that the higher the scatter of LS fibres strength, the higher the hybrid effect.

Simultaneously, an exhaustive work to achieve pseudo-ductile tensile response with UD hybrid composites has been carried out at both the University of Bristol and the Budapest University of Technology and Economics [1, 7, 8, 26-29]. It has been demonstrated that for achieving pseudo-ductility in hybrid composites two damage mechanisms should to take place simultaneously, namely: (i) the fragmentation of the LS material and (ii) the stable delamination of the LS material from the HS material layers close to the LS fractures. In carbon/glass hybrid composites made with prepreg plies, it was shown that, if the carbon layer is thin enough, catastrophic delamination propagation around the first carbon fracture is suppressed and, therefore, further fractures in the carbon layer may occur, introducing pseudo-ductility into the stress–strain curve [1, 27]. According to Jalalvand *et al.* [8], the

fragmentation in the low strain material becomes saturated and stops when there is no longer any part of the low strain material with constant stress. The different failure mechanisms in carbon/glass hybrid composites were found to be dependent on the ratio of carbon to glass thickness and also the absolute thickness of the carbon [26]. As explained in detail by Jalalvand *et al*. [27], the control of the two mentioned factors can lead to four possible tensile damage modes of UD hybrid composites, as described in Section 2.5.3.

An important milestone achieved by Jalalvand *et al*. [8] was the development of an analytical model to predict all possible damage modes of thin-layer UD hybrids. Predictions of this model proved to be in good agreement with nonlinear tensile response of different UD layer-by-layer hybrid configurations. Damage mode maps were generated to study the effects of absolute and relative thicknesses of the carbon layers; these maps have proven to be a very efficient design tool for hybrid composites [27, 28].

In civil engineering context there are already several examples of applying the hybrid composite concept, mainly in the research and development of three main systems: (i) reinforcing bars for reinforced concrete (RC) structures [30-37]; (ii) externally bonded strengthening for RC structures [17, 38-52], and (iii) pultruded profiles for new structures [53-55]. In a general way, experimental results have shown that a significant ductile response, similar or even better, than that of a steel-reinforced concrete member can be achieved with hybrid composites [31, 36]. In addition to gradual failure mode, hybrid composites have the benefit of eliminating the corrosion problems of steel materials [35, 37].

Cui and Tao [35] and Cheung and Tsang [36] conducted works on the development of hybrid composite reinforcing bars. In the design of these solutions four different reinforcing materials, namely carbon, aramid, glass, and steel, were simultaneously used. The resulting hybrid bars demonstrated pseudo-ductile behaviour, with a tensile strength of 644 MPa, a modulus of 140 GPa and an ultimate strain of circa 3%. A series of concrete beams reinforced with the proposed solution were tested and it was demonstrated that the beams had the ability to undergo large inelastic deformations. Pseudo-ductility was found to be similar to that of conventional steel-reinforced beams.

Grace *et al*. [38] develop a UD fabric composed of two types of carbon fibres and one type of glass fibres. In this case, the pseudo-ductility of the composite was achieved through the combination of the different ultimate strain of each of the adopted types of fibres. In [39], the same authors further developed the initial concept by introducing fibres in the diagonal direction, thus enabling the use of the hybrid fabric for simultaneous flexural and shear strengthening of concrete beams. The last work resulted in one US patent [56].

Wu *et al*. [17] developed hybrid composites made of high-strength and high-modulus carbon sheets. The resulting solution was applied in the upgrading of pre-cracked RC beams. It was concluded that the hybrid composites allowed achieving the desired flexural stiffness, 'yielding' strength, and pseudo-ductility.

Several of these attempts (in the field of civil engineering) have been developed/applied without a complete understanding about the behaviour of hybrid composites at material level. In most works, the concept of pseudo-ductility was defined as the successive fractures of different (more than two) reinforcing materials and not as a result of the previously described phenomena of fragmentation and controlled delamination of LS fibres. Moreover, with some exceptions [17, 44, 48, 57, 58], the hybrid effect has been ignored in this set of works and the factors that controlled the damage mode of the hybrid composites have not been clearly explained.

Nowadays, it is very common to apply composites made in-situ through the hand lay-up method, i.e., forming the composite on the surface of the structural member to be strengthened, using flexible dry fibre fabrics or sheets and liquid adhesives. This has proved to be a cost effective method and, in addition, the composite can adopt versatile shapes and sizes using simple tools. Despite its advantages, the hand lay-up method is dependent on the skill of the worker, and thus quality control plays a major role to ensure that defects and voids are avoided. According the best practices suggested in the guidelines, e.g. [59], hand lay-up system shall be referred to the area of dry fibres only because, in this case, final thickness of the composite cannot be deterministically estimated [59].

Due to the above reasons, it is important to study the performance of hybrid composites produced through the hand lay-up method for civil engineering applications. In the context of analytical modelling, Jalalvand *et al*. [8] have proposed a model to predict with proper accuracy the tensile response of hybrid composites made of prepreg systems, cured at controlled conditions of pressure and temperature. In retrofitting and strengthening, resins are usually impregnated by hand into dry fabrics with curing times being governed by the environmental conditions. In fact, this is one of the most widely used processes for manufacturing FRP composites for structural engineering [60]. In this way, the availability of an analytical model to predict the tensile behaviour of hybrid composites, produced by hand lay-up method, is seen as a very important tool for the design of UD hybrid composites in civil engineering context.

The aim of this research is to investigate the tensile stress–strain responses of 16 different UD interlayer (layer-by-layer) hybrid composite combinations, made through the hand lay-up method, of different commercially available raw materials (fibres' packages + resin). Four dry UD fabric materials were used combined with epoxy resin, namely (i) high-modulus carbon, (ii) standard carbon, (iii) E-glass and (iv) basalt, in order to evaluate the hybrid effect and to achieve pseudo-ductility, fully exploiting the benefits of hybridisation. The hybrid effects and

the information of the fibres used in other authors' works, published between 1974 and 2016, were collected with the objective of carrying out a statistical analysis. In this way, the data collection of Manders and Bader [13] and Swolfs *et al*. [4] was updated in this work. The analysis of the obtained experimental results was complemented with analytical modelling based on the approach developed by Jalalvand *et al.* [8] for hybrid composites.

2 EXPERIMENTAL PROGRAM

2.1 Objectives

The main objective of the present work is to contribute to the knowledge on the performance of UD hybrid composites produced by the hand lay-up method. The following specific goals are envisaged:

i. To determine the influence of LS fibres relative volume (vol%) on the hybrid effect of different layer-by-layer hybrid composite combinations made through hand lay-up method;
ii. To understand which non-hybrid properties of the constituent materials influence most the hybrid effect, identifying the correlation between intrinsic mechanical properties of fibres and the obtained response (in the present work, according to general practice [4], failure strains of non-hybrid composite, obtained in tensile tests, were used as the baseline tensile failure strain to compute the hybrid effect);
iii. To evaluate the accuracy of the rule of mixtures (ROM) and of the bilinear ROM to predict respectively the elastic modulus and the tensile strength of the hybrid composites;
iv. To characterize the hybrid pseudo-ductile tensile behaviour;
v. To extend the analytical approach developed by Jalalvand *et al.* [8] to the present experimental program.

2.2 Materials

In the present work, commercial dry UD fabrics with similar areal mass of 400 g/m^2 were used. The materials used for the experiments were the UD HM carbon (S&P C-Sheet 640) [61], ST carbon (S&P C-Sheet 240) [62], E-glass (S&P G-sheet E 90/10) [63], and basalt (Dalla Betta Group U400B-40-50-03) [64] fabrics.

In **Table 1** the density, areal mass, fibre layer thickness (areal mass density divided by the volumetric mass density) and the basic tensile properties of the mentioned materials are presented. The tensile properties of the fibres were determined according ASTM D3379-75 [65]. For each dry fabric, a large number of single fibres (see the details in **Table 1**) were randomly taken from the dry fabrics and tested in tension. The tests were carried out in a Hounsfield H100KS universal testing machine with a maximum load cell capacity of 2.5 N (with an accuracy of ± 0.2% of applied force across load cell force range). Fibres were individually assembled in the tensile jig by

means of a paper template with a fixed gauge length of 20 mm. Fibre ends were glued to the paper template by an ethyl cyanoacrylate-based adhesive. Then the tab ends were gripped in the jaws of the machine. The paper template was cut across, so that just the fibre was fixed as a continuous length within the jig, before starting the tensile tests. The measurements were performed at a rate of 1.5 mm/min, until breakage occurred. For each fibre, records of applied load against extension were taken, and using an average mean diameter, determined through the analysis of microscopy images of fibres obtained with Scanning Electronic Microscopy (SEM), the data were converted to stress against strain.

An epoxy-based material (S&P Resin Epoxy 55) was used as matrix for laminating the studied composites, as recommend by the supplier of three dry fabrics (high-modulus carbon, standard carbon and E-glass). Relatively to basalt fabric, the same resin was used since the corresponding supplier does not provide a package of fibres and resin. According to the supplier, this epoxy has the following main properties [66]: (i) a tensile strength of 35.8 MPa; (ii) a strain at the failure of 2.3%; and, (iii) an elastic modulus of 2.6 GPa.

Each reinforcing material was labelled according to the information included in **Table 1**. In the present work, in case of composite materials, numbers placed after letters are used for indicating number of layers. The order that letters appear indicate the stacking sequence of the reinforcing materials.

2.3 Specimen manufacturing and test setup

The hybrid composite laminates were manufactured by hand lay-up method, following the best practices suggested in the guidelines [59]. Prior to the manufacturing, dry fabrics were cut into 250 mm × 80 mm pieces. A Teflon film was used to avoid the adhesion of the produced composite laminate to the rigid base. The following protocol was used to obtain the laminates: (i) application of a layer of epoxy over the Teflon film with a brush; (ii) saturation of the fabric layer with epoxy resin; (iii) placement of the fabric over last layer, adjusting it manually; (iv) pressure application by means of a ribbed rigid roller, in order to expel both the epoxy resin excess and air in the composite, and also stretching the latter; and (iv) repetition of steps ii to iv for subsequent layers. The top of the laminate was left rough, simulating real applications. All the samples were then cured at room temperature (20 ± 0.5ºC) for 40 days.

The four specimens of each series were obtained from the laminates produced according to the protocol previously described, using a diamond tipped wheel cutter. Tensile tests were performed according to ISO 527-5:2009 standard [67]. Specimen dimensions were 250/150/15/[0.7-3.5]/[0.5-1.0] mm overall length/free length/width/total thickness/fibre layer thickness, respectively.

Aluminium tabs of 50 × 15 mm^2 were used at each end of the specimen to try minimise gripping effects. A clip gauge with a gauge length of 100 mm (with a linear error, including hysteresis of 0.25%) was used.

Tensile tests were carried out at room temperature on a universal testing machine (UTM) equipped with a 200 kN load cell (with a linear error less than 0.05% of full scale) and hydraulic grips, as shown in **Figure 1**. The specimens were held between grips of the UTM and extended (at a rate of 1 mm/min) up to failure.

2.4 Material combinations

In the present work, it was decided to perform single-factor experiments with several levels of LS fibres vol%. Symmetric specimens were adopted to test the hybrid combinations, in order to minimize load eccentricity and differential thermal contraction during the cure of the epoxy resin, ultimately leading to bending-stretching coupling, and thus causing undesirable warping [3]. Furthermore, in a way to try restrict the stress concentrations at the grips, LS layers were whenever possible sandwiched between HS layers, according to Wisnom *et al.* [7] conclusions.

All possible hybrid composite combinations until 5 layers were studied. In total, 16 series were considered: 10 combinations with 3 reinforcing material layers, and 6 combinations with 5 reinforcing material layers. Since each series was composed of 4 specimens, a total of 64 tests were performed. The combinations of 3 symmetrical layers allowed to analyse the following approximate levels of LS fibres vol%: 0%, 33%, 66% and 100%. In addition, combinations with 5 layers allowed to analyse the following approximate levels of LS fibres vol%: 20%, 40% and 60%. It should be noted that specimens with 5 layers were only tested on 2 hybrid combinations: HM carbon/glass and ST carbon/glass. As previously mentioned, the UD fabrics had slightly different nominal thicknesses and, for this reason, the relative volume of LS fibres (*Vol% LS*) was computed in the next sections, according to Equation (1):

$$Vol\%\ LS = \frac{t_L}{t_L + t_H} \times 100 \quad (1)$$

where t_L is the half thickness of the LS layers and t_H is the half thickness of the HS layers.

In **Table 2** the layer ratio and the stacking sequence of the studied hybrid composite combinations are summarized. In addition to hybrid series, 8 series of non-hybrid composites were produced: half with a single layer of reinforcing material and other half with 3 layers of reinforcing material. Each series was composed of 4 specimens, totalling 32 specimens tested.

In the present work, the exact volume of resin was not directly controlled during the application and cross-sectional area of the composite was computed considering only the thickness of the dry fabrics, according the recommendation suggested in the guideline [59]. In this way, mechanical proprieties of impregnated composite (elastic modulus and tensile stress) were computed considering the wet lay-up system similar to an equivalent system of only dry fabrics. However, in order to present an idea of geometric properties, all the composites were measured with a digital calliper (see **Table 3**).

2.5 Analytical models for hybrid composites

2.5.1 Elastic modulus

The longitudinal elastic modulus of the hybrid composites has been shown to follow the linear rule of mixtures (ROM) [4]. According to this model, the elastic modulus of the hybrid composite, E_{hybrid}, can be predicted as the sum of the contributions of the three constituents, given by equation (2):

$$E_{hybrid} = V_L E_L + V_H E_H + V_M E_M \quad (2)$$

where V_L, V_H, V_M, E_L, E_H, and E_M are the volumetric fraction and elastic modulus of the LS fibres, HS fibres and matrix, respectively.

Phillips [14] and Kretsis [16] pointed that some deviations in the predictions of elastic modulus of hybrid composites by using ROM can only be explained by an incorrect use of this rule, namely due to an incorrect input of the volume fraction of reinforcing materials.

In the present work, the linear ROM was used to predict the elastic modulus of hybrid composites in order to check the volume and alignment of the reinforcing materials. To achieve this, the mechanical properties experimentally characterized of non-hybrid composites were used as input variables. The exact volume of resin was not directly controlled during the application and cross-sectional area of the composite was computed considering only the thickness of the dry fabrics, according to the usual practice of the hand lay-up method [59]. In this way, E_L and E_H were considered the elastic modulus of LS and HS one layer composites, respectively. Therefore, the contribution of $V_M E_M$ was contemplated in $V_L E_L$ and $V_H E_H$ terms, leading to $V_L + V_H = 1$ and $V_M E_M = 0$.

2.5.2 Tensile strength

The tensile strength of the hybrid composites do not follow to linear ROM, e.g. [4, 13, 16, 68, 69] because if the volume fraction of HS fibres is appropriate when LS fibres fail, the load can be transferred to HS fibres until their final failure. Otherwise, the composite would fail prematurely. For this reason, some authors [13, 16, 70] have proposed a bilinear ROM (see Eq. (3)) to predict the tensile strength of hybrid composites, σ_{hybrid}.

$$\sigma_{hybrid} = \begin{cases} V_L S_L + V_H E_H \varepsilon_L; \; V_H < V_{crit} \\ V_H S_H; \; V_H > V_{crit} \end{cases} \quad (3)$$

where S_L and S_H are the reference strengths of the LS and HS one layer composites and ε_L is the strain at the failure of the non-hybrid LS composite.

Based on this model, if V_H is lower than the critical value, V_{crit}, the hybrid composite would fail prematurely. On the contrary, if V_H is higher than V_{crit}, hybrid composites would keep their integrity up to the failure of HS fibres.

In the present work, the bilinear ROM model was used to evaluate the magnitude of predictions' errors. V_{crit} was calculated by equating the two branches of equation (3), taking into account that $V_L + V_H = 1$, i.e., V_L is equal to $1\text{-}V_H$:

$$V_{crit} = \frac{S_L}{S_L + S_H - E_H \varepsilon_L} \quad (4)$$

2.5.3 Stress-strain curve

In an UD hybrid composite under uniaxial tension loading conditions, the first damage mode is always the failure of the LS fibres; however, the other following damage modes depend on the properties and configuration of reinforcing materials of the composite [27]. The analytical approach proposed by Jalalvand *et al.* [8] considers that four different damage modes may occur after the LS fibres failure: (i) premature HS failure, (ii) unstable delamination, (iii) LS layer fragmentation and (iv) LS fragmentation and stable delamination. For each hybrid configuration, three stress levels could be computed [8]: (i) the stress at which the first crack in the LS material occurs, $\sigma@LF$, (ii) the stress level at which delamination development occurs, $\sigma@del$, and (iii) the stress when the high strain material fails, $\sigma@HF$, in accordance with the equations (5) to (7), respectively.

$$\sigma@LF = S_L \frac{\alpha\beta + 1}{\alpha(\beta + 1)} \quad (5)$$

$$\sigma@del = \frac{1}{1+\beta} \sqrt{\left(\frac{1+\alpha\beta}{\alpha\beta}\right)\left(\frac{2G_{IIC}E_H}{t_H}\right)} \quad (6)$$

$$\sigma@HF = \frac{1}{(1+\beta)} \frac{S_H}{K_t \sqrt[m_H]{V}} \quad (7)$$

where α and β are the modulus and thickness ratios of the LS to HS fibres, G_{IIC} is the mode II interlaminar fracture toughness of the interface between LS layers and HS layers of the hybrid composite, m_H is the Weibull strength distribution of the modulus of the HS fibres, K_t is the stress concentration factor in the high strain material and V is the volume of the specimen (free length × width × total fibre layer thickness).

Knowing the magnitude of all three possible stresses allows assessing their order of occurrence and, consecutively, the identification of the damage modes, according to **Table 4**. The details of the analytical approach are fully discussed in [8].

After the determination of the damage modes, it is possible to plot the stress–strain curve using the characteristic points given in **Table 5**. In the latter, E_{sat} is the saturated modulus of the composite (according to equation (8)), ε_H is the strain at the failure of the HS fibres and $\varepsilon_{@H\text{-}PS}$ is the strain in the composite at the post-saturation phase when the high strain material fails (according equation (9)).

$$E_{sat} = E_H \frac{\alpha\beta+1}{(\beta+1)(1+\frac{11}{18}\alpha\beta)} \quad (8)$$

$$\varepsilon_{@H-PS} = \frac{\varepsilon_H}{K_t \sqrt[m_H]{V}} - \frac{7}{18}\frac{S_L\beta}{E_H} \quad (9)$$

Since the model by Jalalvand *et al.* [8] does not consider the hybrid effect, the strain at the failure of LS materials in hybrid combination was assumed to be equal to the obtained experimental values (according to the method developed by the author), and S_L was computed according to Hooke's law. In the present work, the definitions of 'yield' stress and pseudo-ductile strain suggested by Jalalvand *et al.* [27] were considered: the 'yield' stress is the stress at the point that response deviates from the initial linear elastic line, i.e., equal to σ@LF and the pseudo-ductile strain is defined as the extra strain between the final failure strain and the strain on the extrapolated initial slope line at the failure stress of the stress-strain diagram (see **Figure 2**).

3 RESULTS AND DISCUSSION

3.1 Tensile properties of non-hybrid composites

In **Figure 3**, the dispersion of the obtained results and their mean values are plotted. It can be concluded that, in all cases, the change from 1 to 3 layers of reinforcing material promotes a reduction of the magnitude of the elastic modulus, tensile strength, and tensile strain at failure. The mean values of the tensile properties and their coefficient of variation (CoV) are presented in **Table 6**, for each series. For each reinforcing material, the *t* statistical test (*t*-test) was used to assess whether the mean values of two groups of tensile properties are statistically different from each other, with a significant level of 5%. The mean values that were significantly different are

underlined in **Table 6**. The highest decreases were founded in glass and HM carbon composites: tensile strength and strain at the failure decreases 416.4 MPa (24.9%) and 675.5 MPa (38.6%) and 0.31% (13.4%) and 0.09% (33.3%), respectively. These decreases can be explained by two factors: (i) for one hand, it is well known that there is a size effect in tensile properties of reinforcing fibre due to the higher probability of finding a cluster of weaker fibre in a larger volume of material [7]; (ii) for other hand, in tensile tests, stress concentrations can be more predominate where the load is introduced. As expected, in the elastic modulus non-significant variations were registered in all cases.

In **Table 6** is even possible to observe, that tensile strength, and consequently the elastic modulus, of cured composites are higher than the obtained values for single fibres. This is due to the fact that, in case of composites, the tensile properties were evaluated considering only the dry fabric thickness which conducted to overestimation of these properties. For other hand, the strain at failure of composites is lower than the one obtained for single fibres. This was expected because in UD composites fibres break as soon as the weakest link is overloaded. Broken fibre sheds load to the nearby fibres, subjecting them to stress concentrations. Stress concentrations increase the failure probability of the nearby fibres that will lead to the development of fibre break clusters and cause final composite failure [71]. Furthermore, in glass and basalt series the mechanical properties of epoxy could be predominant in the composite failure because the strain of the resin at failure is lower than the strain of fibres at failure.

In **Table 6** the obtained failures modes of all specimens are also identified. Each failure mode was labelled according to the information included in ASTM D 3039/D 3039M standard [72]. Numbers placed after letters are used for indicating the number of specimens in which the same failure mode was obtained. As referred before, stress concentrations may be responsible for the variability observed in failure modes and lowering both the average strength and strain. Furthermore, layer overlap, in case of specimens with 3 layers, can lead to the occurrence of more emphasized size effects and different failure modes, such as delamination, that would cause more scatter. Therefore, an accurate way of measuring the strain at failure of non-hybrid composites should be further investigated. For this reason, a hypothetic increase on baseline strain of LS material would lead to a decrease on the values of hybrid effects obtained in the present work. Nevertheless, from **Table 6** it is possible to observe that, for series 1C and 1CHM, 3 out of the 4 tested specimens have failed at gage length.

3.2 Tensile tests of hybrid composites

3.2.1 Elastic modulus and tensile strength

A summary of the tensile properties obtained for the hybrid composites is presented in **Table 7**. Volumes of reinforcing materials were computed as a function of their density and areal mass. The tensile strength was defined as the maximum value observed in the stress–strain curve. The results of 1 layer non-hybrid composites were used to serve as reference in the comparisons with the analytical predictions.

Figure 4 shows the evolution of the elastic modulus with the LS fibre vol% of the tested specimens, as well as the mean and their 95% Fisher level of confidence intervals overlapped with ROM curves. As previously mentioned, the elastic modulus increases linearly with the increase of LS fibres vol%. As expected, the largest elastic modulus increases were found in the combinations of reinforcing materials in which this property differed the most: HM carbon/glass (**Figure 4** (a)) and HM carbon/basalt (**Figure 4** (c)). Relatively to the ST carbon/glass (**Figure 4** (b)), ST carbon/basalt (**Figure 4** (d)), and HM carbon/ST carbon (**Figure 4** (e)) combinations, the elastic modulus increases were softer.

Relatively to ROM, predictions showed a good agreement with the experimental results. The obtained relative errors varying between -14.5% and 9.6%. This magnitude of the error values is acceptable and it is in agreement with the bibliography [16]. For this reason, it is believed that in the present case there was not a significant deviation in fibres alignment. Therefore, it can be stated that ROM is a model that can be used as a quality control tool for hand lay-up hybrid composites, since it allows checking the volume and the alignment of the reinforcing materials used in this type of composites.

Figure 5 presents the experimental results for the case of the tensile strength. As in the previous case, the scatter diagrams of tensile strength results, their mean results, and their 95% Fisher level of confidence intervals were overlapped with bilinear ROM curves. In general, it is possible to distinguish between two types of behaviour: (i) in the combinations that included HM carbon fibres, a small tensile strength variation with increasing LS fibres vol% was registered, and (ii) in the combinations that included ST carbon fibres, a clear tensile strength increase with the increase in LS fibres vol% was observed. This is understandable, since HM carbon exhibits a low tensile strength and, therefore, it is not expectable to observe improvements in the tensile strength by increasing the volume of this material. An opposite behaviour is observed when ST carbon is used.

In the case of bilinear ROM predictions, deviations from the experimental results were also found, varying between -15.7% and 16.9%. In this way, the relative errors were higher than those obtained with ROM. These results were expected, since, as previously explained, the bilinear ROM does not consider delamination and hybrid effect phenomena [8, 69]. In **Figure 5** it is also possible to observe that there were 5 combinations located in the multiple facture zone: 2G/1CHM/2G, 1G/1CHM/1G, 1G/1CHM/1G/1CHM/1G, 1B/1CHM/1B and

1C/1CHM/1C. All these combinations had in common the use of the HM carbon fibres as LS fibres. In these cases, catastrophic failures were avoided. In the remaining cases, a catastrophic failure of the HS fibres occurred at the moment of LS fibres failure. In this way, the bilinear ROM was capable of predicting satisfactorily the occurrence of multiple fractures. This topic is further discussed in Section 3.2.3.

3.2.2 Hybrid effect

The hybrid effect was computed relatively to 1 layer non-hybrid composite results, according to the Equation (10):

$$Hybrid\ effect = \frac{\Delta\varepsilon_L}{\varepsilon_L} \times 100 \quad (10)$$

where $\Delta\varepsilon_L$ is absolute variation of the strain at the failure of LS material obtained in hybrid and non-hybrid composites.

As previously mentioned, volumes of reinforcing materials were adjusted in accordance with their density and areal mass. **Figure 6** shows the scatter diagrams of the obtained hybrid effects, their mean results and their 95% Fisher level of confidence intervals.

As expected, it was possible to observe that the reduction of the LS fibres vol% leads to a clear increase of the hybrid effect. In general, the hybrid effect varied between -14.1% and 44.5%. However, the hybrid effect increase was not linear. In all cases, it was possible to observe that above 60% of relative volume of LS fibres the hybrid effect was close to zero or even negative. As presented above, in non-hybrid composites the use of more layers of the same material caused the reduction of all the analysed tensile properties. The hybrid effect was negative in cases where 2 or 3 layers of LS fibres were used. It should be noted that, since failure strains of 1 layer non-hybrid composite were used as the baseline tensile failure strain to compute the hybrid effect, negative hybrid effects are possible. In fact, it was confirmed that negative hybrid effects never arise when comparisons are made with the results obtained with the 3-layer non-hybrid composites.

Several *t*-tests at a significance level of 5% were performed to compare all pairs of hybrid effect mean values. Relative to HM carbon/glass case, differences between the 3 initial levels of LS fibres vol% hybrid effect mean values were not significant. The same could be concluded for the last 2 levels. The analysis of the carbon/glass series results led to the same conclusion. Since in the remaining combinations of materials only two levels of LS fibres vol% were analysed, the previous conclusion was not refuted for these combinations either.

In order to understand if there were significant variations due to the replacement of glass with basalt material, *t*-tests were performed to compare the pairs of hybrid effect mean values between the combinations of HM carbon/glass, HM carbon/basalt, ST carbon/glass, and ST carbon/basalt. It can be concluded that the changes referred to did not conduct to significant differences in hybrid effect results, as it is shown in **Figure 7**. However, with 38.2% of HM carbon fibres relative volume (1G/1CHM/1G), a significant difference was achieved. From the analysis of **Table 7** it can be seen that for the 1G/1CHM/1G combination the worst prediction of elastic modulus was achieved by ROM, indicating that the mentioned difference was probably promoted by some misalignment of the fibres.

The hybrid effects and the information of the fibres used in other authors' works, published between 1974 and 2016, were contemplated in the present work (see **Table 8**). Although the data collection was mainly focused on the interlayer configurations, the information of intralayer configurations presented by Chamis *et al*. [73] was also included, since it is one of the few works in which the hybrid effect with more than 70% of LS fibres relative volume was studied.

Associations between hybrid effect and material factors (such as S_L, S_H, E_L, E_H, ε_L and ε_H) were analysed by a Spearman's rank test using SPSS version 23 (IBM, New York). Additionally, the hybrid effect was also analysed as function of S_L/S_H, E_L/E_H and $\varepsilon_L/\varepsilon_H$ ratios, S_L-S_H, E_L-E_H and ε_L-ε_H differences and a non-dimensional stiffness parameter, E_{ND}, defined by equation (11). The E_{ND} was first introduced by Swolfs *et al*. [25], who indicated that the hybrid effect depends on this parameter.

$$E_{ND} = \frac{V_L E_L}{V_H E_H} \tag{11}$$

Spearman's correlation coefficient, *r*, is a statistical measure of the "strength" of a monotonic relationship between paired data. In the present work, spearman's rank of data revealed that statistically significant correlations, at a significance level of 5% between the hybrid effect and mentioned variables, were achieved for the cases of S_H, Vol% LS fibres and E_{ND}. There was a weak negative correlation between hybrid effect and S_H (r = - 0.311). On the other hand, moderately strong negative correlations exist between hybrid effect and Vol% LS fibres (r = - 0.526) and E_{ND} (r = - 0.515).

The moderate relationships previously mentioned are plotted in **Figure 8**. The dispersion of results and the low Spearman's correlation coefficients obtained do not allow the suggestion of an appropriate model to describe the results. However, no linear trends are clearly observable in the presented diagrams. It is possible to see in **Figure 8** that the results obtained in the present work are in agreement with those in the literature.

3.2.3 Failure modes

As mentioned before, multiple fractures were achieved in some hybrid configurations, according to bilinear ROM predictions (see **Figure 5**). Usually, multiple fractures in hybrid composites are characterized by 2 successive failures: the LS fibres fail firstly followed by the HS fibres. However, in 4 situations in this work, pseudo-ductile tensile responses with multiple fractures were observed with some combinations that included HM carbon, as it is shown in **Figure 9**. Two outlier results obtained in 1G/1CHM/1G and 1B/1CHM/1B combinations were ignored.

In the case of 2G/1CHM/2G, a mean 'yield' stress of 732.6 MPa and a mean pseudo-ductile strain of 1.4% were registered (see **Figure 9** (a)). In 1C/1CHM/1C combination a mean 'yield' stress of 1504.5 MPa and a mean pseudo-ductile strain of 0.4% were observed (see **Figure 9** (d)). The replacement of glass by basalt resulted in slightly different behaviours (see **Figure 9** (b) and **Figure 9** (c)): with basalt, higher pseudo-ductile strain and 'yield' stress were obtained. The combination with basalt led to a mean 'yield' stress of 1120.7 MPa and a mean pseudo-ductile strain of 2.0%, whereas the combination with glass yielded a mean 'yield' stress of 768.2 MPa and a mean pseudo-ductile strain of 1.2%. Furthermore, two different behaviours were observed: one with (see **Figure 9** (a) and (d)) a clear hardening branch in the end of the pseudo-ductile strain, and another without (see **Figure 9** (b) and (c)) the latter.

It should be noted that, since the strain of the epoxy at failure is lower than the strain of glass and basalt fibres at failure, if a resin with higher ultimate strain had been used, larger pseudo-ductile strains may have been reached in 2G/1CHM/2G, 1G/1CHM/1G and 1B/1CHM/1B combinations. Further studies to confirm these hypotheses are deemed necessary.

In the HM carbon/glass combinations the fragmentation of the HM carbon and delamination could be observed visually during the tensile test due to the translucence of the glass. The specimens were initially black due to the HM carbon natural colour but, after fragmentation and delamination, light was reflected from the interface, and the specimens looked white. **Figure 10** shows an example of the aspect of specimen in consecutive phases of the tensile test. The fragmentation of HM carbon is evident. Furthermore, it is possible to observe localised delamination around the carbon layer fractures that developed stably during test until saturation. It is noticed that each stress-strain curve peak, as it is identified in **Figure 9** (a), corresponds to a crack of the HM carbon and localised delamination.

3.3 Prediction of stress–strain curves

In this section, the predicted stress-strain curves of all hybrid configurations studied in the present work, obtained with the model proposed by Jalalvand *et al*. [8], are compared with the corresponding experimental curves. One layer non-hybrid composite results were used as input variables. Since the model of Jalalvand *et al*. [8] is not able to predict the hybrid effect, the ε_L of the different material combinations was assumed to be equal to the experimental values obtained and S_L was computed according to Hooke's law, a similar procedure was used in [8]. As it was demonstrated, the hybrid effect can increase substantially the strain at failure of LS fibres. For this reason, to turn the model capable of predicting the mechanical behaviour of new configurations, a way to predict the hybrid effect should be incorporated. The length and width of all specimens for prediction of high strain material failure were assumed to be equal to L = 150 mm and W = 15 mm, respectively. The interlaminar toughness, G_{IIC}, for the different hybrid interfaces and the value of the stress concentration factor, K_t, were not experimentally assessed. They were computed in a way that, in combinations with pseudo-ductile behaviour, the fragmentation and dispersed delamination damage mode, indicated in **Table 4**, was analytical achieved. The G_{IIC} was assumed to be constant for the same material combinations. Weibull modulus was assumed to be equal to the value used by Jalalvand *et al*. [8], i.e., m_H = 29.3. The value of the stress concentration factor was assumed constant for all of the specimens, K_t = 0.97. This value is slightly lower than the one used by Jalalvand *et al*. [8] but allowed the best predictions. All input data is shown in **Table 9**.

As it can be seen in **Figure 11** to **Figure 15**, there is a good agreement between predictions and experiments. Analysing the curves, three groups of behaviours can be identified: (i) pseudo-ductile behaviours (the same that were discussed in Section 3.2.3), (ii) failure with two peaks (**Figure 11** (c), **Figure 11** (d) and **Figure 14** (a)), and (iii) premature and abrupt failure of HS fibres (in the remaining cases). The chosen way to estimate the G_{IIC} parameter (considering only configurations in which fragmentation and dispersed delamination damage mode occurred) allowed to estimate with good accuracy the remaining cases.

It is also possible to observe that, in the combinations with pseudo-ductile behaviours, the model was not capable of capturing the peaks in the 'flat-topped stress strain curve', since it considers that the fragmentation and delamination occurred consecutively and not simultaneously. In the 1C/1CHM/1C series, the predicted stress-strain curves was somehow conservative. This occurred because S_L and S_H input properties were probably underestimated because these properties were assumed equal to the experimental values obtained with non-hybrid specimens and there is always some variability in the constituents.

In the 1G/1CHM/1G/1CHM/1G and 1G/3CHM/1G series, the model predicted well the catastrophic delamination damage mode, but the prediction of the delamination branch was much higher than the one observed experimentally. This lack of precision is probably related to some overestimation of G_{IIC} in these cases.

In the case of 1B/1C/1B series, the volume proportion of the constituent materials was between premature failure of HS fibres and catastrophic delamination damage mode. For this reason, the model was not capable of predicting the complete tensile response. A 20% increase in ST carbon thickness, keeping the same volume proportion between the reinforcing materials, was enough to get a correct prediction from the model.

4 CONCLUSIONS

The tensile behaviour of several layer-by-layer hybrid combinations has been investigated using experimental testing and analytical modelling. All the composites were made through the hand lamination of four different commercially available dry UD fabrics: HM carbon (CHM), ST carbon (C), E-glass (G) and basalt (B). The following main observations and conclusions were drawn.

It was verified that hybrid effect depends not only on the vol% of LS fibres but also on the non-dimensional stiffness parameter (E_{ND}), and the elastic modulus of the hybrid composite (E_{hybrid}). According to the Spearman's rank test carried out, moderately strong negative correlations between hybrid effect and Vol% LS fibres (r = - 0.526) and E_{ND} (r = - 0.515) were found. The hybrid effect varied between -14.1% and 44.5%. The maximum hybrid effect was obtained combining HM carbon with carbon, in combination 1C/1CHM/1C, and the minimum was obtained combining HM carbon with glass, in combination 1G/3CHM/1G. In all analysed cases, it was possible to observe that above 60% of LS fibres relative volume, the hybrid effects were nearly zero or negative. It is believed that the latter results are due to the size effect, since in the present work hybrid effects were computed in respect to 1 layer non-hybrid composite results, and in the cases in which the negative hybrid effect were obtained 2 or 3 layers of LS fibres were used. In this way, the magnitude of the hybrid effect potentially depends on the ply thickness of the LS fibres and this subject should be further studied.

Elastic modulus was well-predicted using the rule of mixtures (ROM). The obtained relative errors were acceptable, varying between -14.5% and 9.6%. In the case of the tensile strength, the relative errors between the bilinear ROM prediction and experimental results varied between -15.7% and 16.9%. In this case, larger errors were expected comparatively with elastic modulus predictions, since bilinear ROM does not account for the hybrid effect and size effect. However, the bilinear ROM was capable of predicting satisfactorily for the cases where multiple fractures occurred.

In the four tested hybrid combinations, that included HM carbon as LS material (2G/1CHM/G, 1G/1CHM/1G, 1B/1CHM1B, and 1C/1CHM/1C), pseudo-ductile tensile responses with fragmentation and dispersed delamination were achieved. In these combinations, the mean 'yield' stress varied between 732.6 and 1504.5 MPa and the pseudo-ductile strain between 0.4 and 2.0%.

The analytical approach developed by Jalalvand *et al*. [8] allowed to predict all the failure modes successfully. In this way, the presented work validated the developed approach for the set of materials and fabrication method used. However, since the hybrid effect can increase substantially the strain at failure of LS fibres, it is recommend to incorporate a way of predicting the hybrid effect into the model in the future.

Acknowledgments

The authors wish to thank to FCT - Portuguese Foundation for Science and Technology and to the Doctoral Program Eco-Construction and Rehabilitation for supporting the PhD grant (PD/BD/52660/2014). Acknowledgements are extended to the following programs that partially supported the study herein presented: European Funds for Regional Development (FEDER) through the Operational Program for Competitiveness Factors (COMPETE), Operational Program for Competitiveness and Internationalization (POCI), and again FCT through both FRPLongDur POCI-01-0145-FEDER-016900 (FCT reference PTDC/ECM-EST/1282/2014) and POCI-01-0145-FEDER-007633 projects. The authors also acknowledge the support of S&P Clever Reinforcement Ibérica Lda and the Dalla Betta Group Company. Last but not least, the contributions of Professor Sandra Nunes in early stages of experimental campaign is gratefully acknowledged.

REFERENCES

[1] G. Czél, M.R. Wisnom, Demonstration of pseudo-ductility in high performance glass/epoxy composites by hybridisation with thin-ply carbon prepreg, Composites: Part A: Applied Science and Manufacturing 52 (2013) 23–30.
[2] G. Czél, M. Jalalvand, M.R. Wisnom, T. Czigány, Design and characterisation of high performance, pseudo-ductile all-carbon/epoxy unidirectional hybrid composites., Composites Part B 111 (2017) 348-356.
[3] J. Summerscales, D. Short, Carbon fibre and glass fibre hybrid reinforced plastics, Composites 9(3) (1978) 157–66.
[4] Y. Swolfs, L. Gorbatikh, I. Verpoest, Fibre hybridisation in polymer composites: a review, Composites Part A: Applied Science and Manufacturing 67 (2014) 181-200.
[5] G. Marron, S. Fisher, F.R. Tuler, H.D. Wagner, Hybrid effects in composites: conditions for positive or negative effects versus rule-of-mixtures behaviour Journal of Materials Science 13(7) (1978) 1419–26.
[6] T. Hayashi, On the improvement of mechanical properties of composites by hybrid composition., Proc 8th Intl Reinforced Plastics Conference. (1972) 149-152.
[7] M.R. Wisnom, G. Czél, Y. Swolfs, M. Jalalvand, L. Gorbatikh, I. Verpoest, Hybrid effects in thin ply carbon/glass unidirectional laminates: Accurate experimental determination and prediction, Composites: Part A 88 (2016) 131–139.

[8] M. Jalalvand, G. Czél, M.R. Wisnom, Damage analysis of pseudo-ductile thin-ply UD hybrid composites – A new analytical method, Composites: Part A 69 (2015) 83–93.
[9] L.N. Phillips, Improving racing-car bodies, Composites 1 (1969) 50-51.
[10] C. Zweben, Tensile strength of hybrid composites, Journal of Materials Science 12 (1977) 1325-1337.
[11] J.N. Kirk, M. Munro, P.W.R. Beaumont, The fracture energy of hybrid carbon and glass fibre composites, Journal of Materials Science (1978) 2197-2204.
[12] N.L. Hancox, H. Wells, Aluminum/Carbon Fiber Hybrid Composites, Polymer Engineering and Sience 19(13) (1979).
[13] P.W. Manders, M.G. Bader, The strength of hybrid glass/carbon fibre composites - Part 1, Journal of Materials Science 16 (1981) 2233-2245.
[14] M.G. Phillips, Composition parameters for hybrid composite materials, Composites 12(2) (1981) 113-6.
[15] B.G. Harlow, Statistical Properties of Hybrid Composites. I. Recursion Analysis, Proc. R. Soc. Lond. A 389 (1983) 67-100.
[16] G. Kretsis, A review of the tensile, compress,ve, flexural and shear properties of hybrid fibre reinforced plastics., Composites 18(1) (1987).
[17] Z. Wu, Y. Shao, K. Iwashita, K. Sakamoto, Strengthening of Preloaded RC Beams Using Hybrid Carbon Sheets, J. Compos. Constr. 11 (2007) 299-307.
[18] Y. Swolfs, L. Gorbatikh, V. Romanov, S. Orlova, S.V. Lomov, I. Verpoest, Stress concentrations in an impregnated fibre bundle with random fibre packing, Composites Science and Technology 74 (2013) 113–120.
[19] Y. Swolfs, L. Gorbatikh, I. Verpoest, Stress concentrations in hybrid unidirectional fibre-reinforced composites with random fibre packings, Composites Science and Technology 85 (2013) 10–16.
[20] Y. Swolfs, G. Czél, M. Jalalvand, M. Wisnom, I. Verpoest, L. Gorbatikh, Model validation of the hybrid effect in carbon/glass hybrid composites, 7th International Conference on Composites Testing and Model Identification, IMDEA, 2015 (2015).
[21] Y. Swolfs, R.M. McMeeking, I. Verpoest, L. Gorbatikh, The effect of fibre dispersion on initial failure strain and cluster development in unidirectional carbon/glass hybrid composites, Composites: Part A 69 (2015) 279–287.
[22] Y. Swolfs, R.M. McMeeking, I. Verpoest, L. Gorbatikh, Matrix cracks around fibre breaks and their effect on stress redistribution and failure development in unidirectional composites, Composites Science and Technology 108 (2015) 16–22.
[23] Y. Swolfs, I. Verpoest, L. Gorbatikh, Issues in strength models for unidirectional fibre-reinforced composites related to Weibull distributions, fibre packings and boundary effects, Composites Science and Technology 114 (2015) 42–49.
[24] Y. Swolfs, I. Verpoest, L. Gorbatikh, Maximising the hybrid effect in unidirectional hybrid composites, Materials and Design 93 (2016) 39–45.
[25] Y. Swolfs, R.M. McMeeking, V.P. Rajan, F.W. Zok, I. Verpoest, L. Gorbatikh, Global load-sharing model for unidirectional hybrid fibre-reinforced composites., Journal of the Mechanics and Physics of Solids 84 (2015) 380–394.
[26] M. Jalalvand, G. Czél, M.R. Wisnom, Numerical modelling of the damage modes in UD thin carbon/glass hybrid laminates, Composites Science and Technology 94 (2014) 39–47.
[27] M. Jalalvand, G. Czél, M.R. Wisnom, Parametric study of failure mechanisms and optimal configurations of pseudo-ductile thin-ply UD hybrid composites, Composites: Part A 74 (2015) 123–131.
[28] G. Czél, M. Jalalvand, M.R. Wisnom, Design and characterisation of advanced pseudo-ductile unidirectional thin-ply carbon/epoxy–glass/epoxy hybrid composites, Composite Structures 143 (2016) 362–370.
[29] H. Yu, M.L. Longana, M. Jalalvand, M.R. Wisnom, K.D. Potter, Pseudo-ductility in intermingled carbon/glass hybrid composites with highly aligned discontinuous fibres, Composites: Part A 73 (2015) 35–44.
[30] V. Tamuzs, R. Tepfers, Ductility of non-metallic hybrid fiber composite reinforcement for concrete., Proceedings of the Second International RILEM Symposium,Ghent, Belgium. August. (1996).
[31] H.G. Harris, W. Somboonsong, F.K. Ko, New ductile Hybrid FRP reinforcing bar for concrete structures., J. Compos. Constr. 2 (1998) 28-37.
[32] C.E. Bakis, J.A. Terosky, A. Nanni, S.W. Koehler, Self-monitoring, pseudo-ductile, hybrid FRP reinforcement rods for concrete applications., Composite Science Technology 61 (2001) 815-823.
[33] A. Belarbi, S.E. Watkins, K. Chandrashekhara, J. Corra, B. Konz1, Smart fiber-reinforced polymer rods featuring improved ductility and health monitoring capabilities, Smart Mater. Struct. 10 (2001) 427–431.
[34] J.-P. Won, Chan-Gi Park, C.-I. Jang, Tensile Fracture and Bond Properties of Ductile Hybrid FRP Reinforcing Bars, Polymers & Polymer Composites 15(1) (2007).
[35] Y.-H. Cui, J. Tao, A new type of ductile composite reinforcing bar with high tensile elastic modulus for use in reinforced concrete structures, Can. J. Civ. Eng. 36 (2009) 672–675.

[36] M.M.S. Cheung, T.K.C. Tsang, Behaviour of Concrete Beams Reinforced with Hybrid FRP Composite Rebar, Advances in Structural Engineering 13 (2010).
[37] B. Behnam, C. Eamon, Resistance Factors for Ductile FRP-Reinforced Concrete Flexural Members., Journal of Composites for Construction. doi:10.1061/(ASCE)CC.1943-5614.0000363 (2013).
[38] N.F. Grace, G. Abdel-Sayed, W.F. Ragheb, Strengthening of Concrete Beams Using Innovative Ductile Fiber-Reinforced Polymer Fabric, ACI Structural Journal 103(5)(99(5)) (2002) 672–700.
[39] N.F. Grace, W.F. Ragheb, G. Abdel-Sayed, Development and application of innovative triaxially braided ductile FRP fabric for strengthening concrete beams, Composite Structures 64 (2004) 521–530.
[40] N. Attari, S. Amziane, M. Chemrouk, Flexural strengthening of concrete beams using CFRP, GFRP and hybrid FRP sheets, Construction and Building Materials 37 (2012) 746–757.
[41] A. Hosny, H. Shaheen, A. Abdelrahman, T. Elafandy, Performance of reinforced concrete beams strengthened by hybrid FRP laminates, Cement & Concrete Composites 28 (2006) 906–913.
[42] R.A. Hawileh, H.A. Rasheed, J.A. Abdalla, A.K. Al-Tamimi, Behavior of reinforced concrete beams strengthened with externally bonded hybrid fiber reinforced polymer systems, Materials and Design 53 (2014) 972–982.
[43] T.H.-K. Kang, W. Kim, S.-S. Ha, D.-U. Choi, Hybrid Effects of Carbon-Glass FRP Sheets in Combination with or without Concrete Beams, International Journal of Concrete Structures and Materials Vol.8, No.1, pp.27–41, March 2014 DOI 10.1007/s40069-013-0061-0 (2014).
[44] P. Zhang, H. Zhu, G. Wu, S. Meng, Z. Wu, Flexural Performance of HFRP-RC Composite T-Beams with Different Interfaces, J. Compos. Constr., 04016101 (2016).
[45] H. Nikopour, M. Nehdi, Shear repair of RC beams using epoxy injection and hybrid external FRP, Materials and Structures 44 (2011) 1865–187.
[46] G. Wu, Z.S. Wu, Z.T. Lu, Y.B. Ando, Structural Performance of Concrete Confined with Hybrid FRP Composites, Journal of reinforced plastics and composites 27(12) (2008).
[47] A.D. Luca, F. Nardone, F. Matta, A. Nanni, G.P. Lignola, A. Prota, Structural Evaluation of Full-Scale FRP-Confined Reinforced Concrete Columns, J. Compos. Constr 15 (2011) 112-123.
[48] S. Xu, L. Li, Y. Guo, Study on experimental behavior of concrete circular column confined by HFRP under axial compression, Advanced Materials Research 450-451 (2012) 491-494.
[49] L.-J. Li, S.-D. Xu, L. Zeng, Y.-C. Guo, Study on mechanical behavior of circular concrete columns confined by HFRP under axial compressive load, Research and Applications in Structural Engineering, Mechanics and Computation – Zingoni (Ed.) Taylor & Francis Group, London, ISBN 978-1-138-00061-2 (2013).
[50] J. Li, B. Samali, L. Ye, S. Bakoss, Behaviour of concrete beam–column connections reinforced with hybrid FRP sheet, Composite Structures 57 (2002) 357–365.
[51] J. Li, S.L. Bakoss, B. Samali, L. Ye, Reinforcement of concrete beam-column connections with hybrid FRP sheet, Composite Structures 47 (1999) 805-812.
[52] N. Attari, S. Amziane, M. Chemrouk, Efficiency of Beam–Column Joint Strengthened by FRP Laminates, Advanced Composite Materials 19 (2010) 171–183.
[53] S.R.P.R. Mantena, Axial Loading and Buckling Response Characteristics of Pultruded Hybrid Glass-Graphite/Epoxy Composite Beams, Journal of Reinforced Plastics and Composites 22(7) (2003).
[54] W.F. Ragheb, Hybridization Effectiveness in Improving Local Buckling Capacity of Pultruded I-Beams, Mechanics of Advanced Materials and Structures 17 (2010) 448–457.
[55] F. Nunes, J.R. Correia, N. Silvestre, Structural behaviour of hybrid FRP pultruded columns. Part 1: Experimental study, Composite Structures 139 (2016) 291–303.
[56] N.F. Grace, W.F. Ragheb, G. Abdel-Sayed, Ductile Hybrid Structural Fabric, Patent No.: US 6,790,518 B2 (2002).
[57] T.H.-K. Kang, W. Kim, S.-S. Ha, D.-U. Choi, Hybrid Effects of Carbon-Glass FRP Sheets in Combination with or without Concrete Beams, International Journal of Concrete Structures and Materials 8(1) (2014) 27–41.
[58] G. Wu, J.-W. Shi, W.-J. Jing, Z.-S. Wu, Flexural Behavior of Concrete Beams Strengthened with New Prestressed Carbon-Basalt Hybrid Fiber Sheets, Journal Of Composites For Construction, 18. ISSN 1090-0268/04013053(10) (2014).
[59] CNR-DT200, Guide for the Design and Construction of Externally Bonded FRP Systems for Strengthening Existing Structures. Advisory Committee on Techincal Recommendations for Construction, National Research Council, Rome, Italy, (2013).
[60] L. Bank, Composites for Construction - Structural Design with FRP Materials, John Wiley & Sons, Inc. (2006).
[61] S&P, Technical Data Sheet S&P C-Sheet 640, (2015).
[62] S&P, Technical Data Sheet S&P C-Sheet 240, (2015).
[63] S&P, Technical Data Sheet S&P G-Sheet E or AR 90/10, typA, (2015).
[64] Dalla-Betta-group, Catalogue 2015, (2015).

[65] ASTM, D 3379 – 75 - Standard Test Method for Tensile Strength and Young's Modulus for High-Modulus Single-Filament Materials., 1989.
[66] S&P, Technical Data Sheet S&P Resin 55, (2015).
[67] ISO, 527-5 Plastics — Determination of tensile properties; Part 5: Test conditions for unidirectional fibre-reinforced plastic composites. EUROPEAN COMMITTEE FOR STANDARDIZATION, (2009).
[68] N. Pan, R. Postle, The tensile strength of hybrid fibre composites: a probabilist analysis of hybrid effects, Phil. Trans. R. Soc. Lond. A 354 (1996) 1875-1897.
[69] Y. Shan, K. Liao, Environmental fatigue behavior and life prediction of unidirectional glass–carbon/epoxy hybrid composites, International Journal of Fatigue 24 (2002) 847–859.
[70] J. Aveston, J.M. Sillwood, Synergistic fibre strengthening in hybrid composites, Journal of Materials Science 11(1877-1883) (1976).
[71] Y. Swolfs, I. Verpoest, L. Gorbatikh, A review of input data and modelling assumptions in longitudinal strength models for unidirectional fibre-reinforced composites, Composite Structures 150 (2016) 153–172.
[72] ASTM, D 3039/D 3039M Standard Test Method for Tensile Properties of Polymer Matrix Composite Materials, (2002).
[73] C.C. Chamis, R.F. Lark, J.H. Sinclair, Mechanical property characterization of intraply hybrid composites, NASA Technical Memorandum 79306 (1979).
[74] I. Taketa, J. Ustarroz, L. Gorbatikh, S.V. Lomov, I. Verpoest, Interply hybrid composites with carbon fiber reinforced polypropylene and self-reinforced polypropylene, Composites: Part A 41 (2010) 927–932.
[75] K.S. Pandya, C. Veerraju, N.K. Naik, Hybrid composites made of carbon and glass woven fabrics under quasi-static loading, Materials and Design 32 (2011) 4094–4099.
[76] J. Shi, H. Zhu, Z. Wu, G. Wu, Durability of BFRP and hybrid FRP sheets under Freeze-Thaw Cycling, Advanced Materials Research 163-167 (2011) 3297-3300.
[77] Y. Zhang, Y. Li, H. Ma, T. Yu, Tensile and interfacial properties of unidirectional flax/glass fiber reinforced hybrid composites., Composites Science and Technology 88 (2013) 172–177.
[78] J.-W. Shi, H. Zhu, G. Wu, Z.-S. Wu, Tensile behavior of FRP and hybrid FRP sheets in freeze–thaw cycling environments, Composites: Part B 60 (2014) 239–247.
[79] I.D.G.A. Subagia, Y. Kim, L.D. Tijing, C.S. Kim, H.K. Shon, Effect of stacking sequence on the flexural properties of hybrid composites reinforced with carbon and basalt fibers., Composites: Part B 58 (2014) 251–258.
[80] M.H. Ikbal, A. Ahmed, W. Qingtao, Z. Shuai, L. Wei, Hybrid composites made of unidirectional T600S carbon and E-glass fabrics under quasi-static loading., Journal of Industrial Textiles 0(00) (2016) 1–25.

List of Tables

Table 1 — Properties of the dry fabrics and tensile properties of fibres.

Material ID	**Properties of the dry fabric, as reporter by the manufacturer**				**Properties of the fibres (tested according to ASTM D3379)**			
	Density [g/m^3]	**Areal mass** [g/m^2]	**Fibre layer thickness** [mm/layer]	**N. of samples**	**Fibre diameter** [μm] (CoV [%])	**Elastic modulus** [GPa] (CoV [%])	**Tensile strength** [MPa] (CoV [%])	**Strain at the failure** [%] (CoV [%])
Basalt (B)	2.67	420	0.157	50	18.14 (3.56)	61.41 (31.14)	1886.70 (40.79)	3.10 (27.73)
E-glass (G)	2.60	400	0.154	50	14.98 (16.25)	76.92 (27.97)	2662.06 (33.88)	3.72 (20.45)
ST carbon (C)	1.79	400	0.223	36	7.88 (5.15)	213.95 (43.36)	3920.67 (39.37)	1.38 (17.37)
HM carbon (CHM)	2.10	400	0.190	26	11.03 (6.66)	558.07 (24.67)	2934.24 (19.16)	0.53 (18.99)

Table 2 — Layer ratio and stacking sequence of the tested hybrid composites.

Designation	**Layer ratio (LS/HS fibres)** [%]	**Stacking sequence**
1LS/1HS/1LS	66/33	☐■☐
1HS/3LS/1HS	60/40	■☐☐☐■
1HS/1LS/1HS/1LS/1HS	40/60	■☐■☐■
1HS/1LS/1HS	33/66	■☐■
2HS/1LS/2HS	20/80	■■☐■■

Notes: ■ – HS fibres layer; ☐ – LS fibres layer.

Table 3 — Geometric properties of specimens.

Material combination	**Series ID**	**Total thickness** [mm] (CoV [%])	**Fibre layer thickness** [mm]	**HS layer thickness** [mm]	**LS layer thickness** [mm]	**Fibre volume fraction** [%]
Non-hybrid	1B	1.01 (18.43)	0.157	--	--	15.57
	3B	1.90 (11.89)	0.471	--	--	24.80
	1G	0.66 (12.74)	0.154	--	--	23.27
	3G	1.87 (3.42)	0.462	--	--	24.67
	1C	1.22 (11.30)	0.223	--	--	18.27
	3C	2.46 (0.85)	0.669	--	--	27.16
	1CHM	1.31 (7.93)	0.190	--	--	14.49
	3CHM	2.95 (9.82)	0.570	--	--	19.34
C/B	1C/1B/1C	2.62 (4.82)	0.603	0.157	0.446	23.01
	1B/1C/1B	2.07 (6.02)	0.537	0.314	0.223	25.92
CHM/B	1CHM/1B/1CHM	2.37 (7.99)	0.537	0.157	0.380	22.71
	1B/1CHM/1B	2.28 (7.96)	0.504	0.314	0.190	22.09
CHM/C	1CHM/1C/1CHM	2.56 (5.55)	0.603	0.223	0.380	23.55
	1C/1CHM/1C	2.55 (4.36)	0.636	0.446	0.190	24.98
C/G	1C/1G/1C	2.85 (7.61)	0.600	0.154	0.446	21.04
	1G/3C/1G	3.24 (6.27)	0.977	0.308	0.669	30.19
	1G/1C/1G/1C/1G	3.05 (3.52)	0.908	0.462	0.446	29.73
	1G/1C/1G	2.05 (4.74)	0.531	0.308	0.223	25.87
	2G/1C/2G	2.91 (3.47)	0.839	0.616	0.223	28.88
CHM/G	1CHM/1G/1CHM	2.66 (5.94)	0.534	0.154	0.380	20.11
	1G/3CHM/1G	3.48 (3.69)	0.878	0.308	0.570	25.25
	1G/1CHM/1G/1CHM/1G	3.36 (2.59)	0.842	0.462	0.380	25.10
	1G/1CHM/1G	2.13 (3.29)	0.498	0.308	0.190	23.40
	2G/1CHM/2G	3.02 (4.00)	0.806	0.616	0.190	26.65

Table 4 — Summary of different damage modes in function of stress level (adapted from [27]).

Damage mode	**Stress level**
Premature failure	$\sigma@HF \leq \sigma@LF \leq \sigma@del$
	$\sigma@HF \leq \sigma@del \leq \sigma@LF$
Catastrophic delamination	$\sigma@del \leq \sigma@HF \leq \sigma@LF$
	$\sigma@del \leq \sigma@LF \leq \sigma@HF$
Fragmentation	$\sigma@LF \leq \sigma@HF \leq \sigma@del$
Fragmentation & dispersed delamination	$\sigma@LF \leq \sigma@del \leq \sigma@HF$

Table 5 — Characteristic points of different damage processes on stress–strain graph (adapted from [8]).

Damage mode	Point 1	Point 2	Point 3	Point 4	Point 5
Premature failure	(0,0)	$(\varepsilon_L, \sigma@LF)$			
Catastrophic delamination	(0,0)	$(\varepsilon_L, \sigma@LF)$	$(\varepsilon_L, \sigma@del)$	$\left(\frac{\sigma@del(1+\beta)}{E_H}, \sigma@del\right)$	$\left(\frac{\varepsilon_H}{K_t \sqrt[m_H]{V}}, \sigma@HF\right.$
Fragmentation	(0,0)	$(\varepsilon_L, \sigma@LF)$	$\left(\frac{\sigma@LF}{E_{sat}}, \sigma@LF\right)$	$(\varepsilon_{H-PS}, \sigma@HF)$	
Fragmentation & dispersed delamination	(0,0)	$(\varepsilon_L, \sigma@LF)$	$\left(\frac{\sigma@LF}{E_{sat}}, \sigma@LF\right)$	$\left(\frac{\sigma@del(1+\beta)}{E_H}, \sigma@del\right)$	$\left(\frac{\varepsilon_H}{K_t \sqrt[m_H]{V}}, \sigma@HF\right.$

Table 6 — Tensile properties obtained with non-hybrid composites.

Series ID	**Elastic modulus** [GPa] (CoV [%])	**Tensile strength** [MPa] (CoV [%])	**Strain at the failure** [%] (CoV [%])	**Failure modes, according to ASTM D3039** [72]
1B	102.5 (15.46)	2244.2 (20.17)	2.46 (10.61)	LIT(1) OGM(3)
3B	92.6 (13.55)	1974.6 (15.76)	2.40 (8.26)	OGM(4)
1G	81.6 (7.39)	1671.2 (8.59)	2.31 (3.78)	LGM(2)
3G	80.6 (10.10)	1254.8 (15.05)	2.00 (13.95)	LAT(1) LGM(2) AGM(1)
1C	231.3 (12.50)	2565.9 (10.18)	1.09 (8.81)	OGM(1) LGM(3)
3C	227.6 (5.80)	2363.2 (7.44)	1.02 (6.02)	LAB(1) LGM(1) LIT(1) LAT(1)
1CHM	624.1 (11.13)	1749.4 (24.39)	0.27 (19.61)	LGM(3) SGM(1)
3CHM	588.2 (3.97)	1073.9 (18.27)	0.18 (15.84)	LAB(3) LIT(1)

Note: the pair mean values underlined are significantly different from each other (according to t-test); L – lateral; S – longitudinal splitting; O – other; I – inside grip; G – gage; A – at grip; T – top; M – middle; B – bottom; numbers placed after letters are used for indicating the number of specimens in which the same failure mode was obtained.

Table 7 — Tensile properties obtained with the hybrid composites and ROM and bilinear ROM predictions.

Material combination	Series ID	Volume of LS fibres [%]	Elastic modulus			Tensile strength			Strain at the failure of LS fibres [%] (CoV [%])	Hybrid effect [%]	Failure modes, according ASTM D3039 [72]
			Experimental [GPa] (CoV [%])	ROM [GPa]	Relative error [%]	Experimental [MPa] (CoV [%])	Bilinear ROM [MPa]	Relative error [%]			
C/B	1C/1B/1C	74.0	218.4 (2.84)	197.7	9.5	2191.4 (7.28)	2189.3	0.1	0.99 (5.76)	-8.99	LAT(4)
	1B/1C/1B	41.5	152.5 (5.93)	155.9	-2.2	1950.2 (7.51)	1718.4	11.9	1.28 (3.46)	17.37	OGM(4)
CHM/B	1CHM/1B/1CHM	70.8	474.1 (2.25)	471.6	0.5	1150.0 (14.10)	1325.4	-15.3	0.24 (11.19)	-12.95	LAT(3) LGM(1)
	1B/1CHM/1B	37.7	297.4 (9.29)	299.1	-0.6	1328.0 (10.74)	1398.1	-5	0.36 (5.77)	30.19	fragmentation
CHM/C	1CHM/1C/1CHM	63.0	489.6 (7.39)	478.8	2.2	1352.5 (5.10)	1350.3	0.2	0.27 (5.55)	-1.50	LGM(1) LAB(1) LAT(2)
	1C/1CHM/1C	29.5	368.8 (6.43)	348.6	5.5	1937.5 (6.79)	1809.0	7	0.39 (3.59)	44.52	fragmentation
C/G	1C/1G/1C	74.3	201.7 (9.63)	192.8	4.4	2176.9 (8.55)	2135.1	1.9	1.04 (1.92)	-4.44	LAB(3) LAT(1)
	1G/3C/1G	68.5	202.4 (2.64)	184.0	9.6	2216.0 (8.77)	2037.8	8.0	1.08 (6.26)	-0.20	LAB(2) LIT(1) LGM(1)
	1G/1C/1G/1C/1G	49.1	148.9 (11.75)	155.1	-4.1	1776.3 (10.55)	1712.6	3.6	1.19 (3.68)	9.15	LAT(1) LGM(2) LAB(1)
	1G/1C/1G	42.0	146.7 (5.92)	144.4	1.6	1856.0 (5.67)	1593.6	14.1	1.27 (2.72)	16.33	LGM(4)
	2G/1C/2G	26.6	110.8 (10.21)	121.4	-9.5	1244.4 (1.74)	1335.4	-7.3	1.18 (8.27)	7.33	LAT(2) LAB(1) LGM(1)
CHM/G	1CHM/1G/1CHM	71.2	454.5 (11.95)	457.7	-2.9	1168.9 (19.49)	1313.7	-12.4	0.25 (11.66)	-7.07	LAT(2) LAB(1) LGM(1)
	1G/3CHM/1G	64.9	439.2 (7.35)	433.8	-0.6	1053.5 (10.14)	1218.4	-15.7	0.23 (6.43)	-14.09	LGM(1) LAT(2) LAB(1)
	1G/1CHM/1G/1CHM/1G	45.1	318.7 (7.33)	326.4	-2.4	1105.8 (9.18)	918.9	16.9	0.35 (5.02)	27.66	LGM(2) LAT(2)
	1G/1CHM/1G	38.2	252.0 (8.55)	288.6	-14.5	1054.7 (9.11)	1032.8	2.0	0.30 (2.39)	9.97	fragmentation
	2G/1CHM/2G	23.6	214.3 (8.45)	209.5	2.2	1164.7 (14.47)	1276.8	-10.0	0.33 (14.65)	21.94	fragmentation

Notes: L – lateral; S – longitudinal splitting; O – other; I – inside grip; G – gage; A – at grip; T – top; M – middle; B – bottom; numbers placed after letters are used for indicating the number of specimens in which the same failure mode was obtained.

Table 8 — Resume of tensile properties of different hybrid combinations obtained by different authors.

Year	Ref.	Matrix	Stacking sequence	Tensile strength [MPa]	Elastic modulus [GPa]	Strain at the failure [%]	S_L	E_L	ε_L	S_H	E_H	ε_H	Vol% LS [%]	Hybrid effect [%]
1974	[13]	Epoxy	1G/2C/1G	300	89	0.37	400.00	142.00	0.26	520.00	41.00	1.25	50.0	42.0
1974		Epoxy	1G/1C/1G	340	72	0.48	400.00	142.00	0.26	520.00	41.00	1.25	33.0	85.0
1976		Vinylester	4G/1C	660	56	1.18	1130.00	115.00	0.98	730.00	40.00	2.00	20.0	20.0
1976		Vinylester	3G/1C	690	60	1.15	1130.00	115.00	0.98	730.00	40.00	2.00	25.0	17.0
1976		Vinylester	2G/1C	720	65	1.11	1130.00	115.00	0.98	730.00	40.00	2.00	33.0	13.0
1976		Vinylester	1G/1C	750	75	1.00	1130.00	115.00	0.98	730.00	40.00	2.00	50.0	2.0
1977		Epoxy	1C/1G						1.80			1.04	50.0	3.8
1978		Epoxy	1C/1G	850	61	1.39	1200.00	97.00	1.23	700.00	25.00	2.80	50.0	13.0
1979		Epoxy	2C/2G	830	61	1.36	1200.00	97.00	1.23	700.00	25.00	2.80	50.0	11.0
1980		Epoxy	5C/5G	800	62	1.29	1200.00	97.00	1.23	700.00	25.00	2.80	50.0	5.0
1981		Epoxy	1G/1CHS/1G	1040	83	1.25	1520.00	135.00	1.12	1200.00	39.00	3.00	33.0	39.0
1981		Epoxy	2G/1CHS/2G	920	65	1.42	1520.00	135.00	1.12	1200.00	39.00	3.00	20.0	57.0
1981		Epoxy	3G/1CHS/3G	870	59	1.48	1520.00	135.00	1.12	1200.00	39.00	3.00	14.0	67.0
1981		Epoxy	4G/1CHS/4G	900	60	1.49	1520.00	135.00	1.12	1200.00	39.00	3.00	11.0	74.0
1981		Epoxy	6G/1CHS/6G	820	55	1.5	1520.00	135.00	1.12	1200.00	39.00	3.00	8.0	82.0
1981		Epoxy	9G/1CHS/9G	760	49	1.55	1520.00	135.00	1.12	1200.00	39.00	3.00	5.0	88.0
1981		Epoxy	2G/2CHS/2G	1030	76	1.35	1520.00	135.00	1.12	1200.00	39.00	3.00	33.0	40.0
1981		Epoxy	3G/2CHS/3G	970	72	1.35	1520.00	135.00	1.12	1200.00	39.00	3.00	25.0	50.0
1981		Epoxy	1G/3CHS/1G	1430	104	1.37	1520.00	135.00	1.12	1200.00	39.00	3.00	60.0	18.0

Table 8 — (Continued)

Year	Ref.	Matrix	Stacking sequence	Tensile strength [MPa]	Elastic modulus [GPa]	Strain at the failure [%]	S_L	E_L	ε_L	S_H	E_H	ε_H	Vol% LS [%]	Hybrid effect [%]
1981	[13]	Epoxy	3G/3CHS/3G	1040	77	1.36	1520.00	135.00	1.12	1200.00	39.00	3.00	33.0	40.0
1981		Epoxy	8G/3CHS/8G	820	58	1.41	1520.00	135.00	1.12	1200.00	39.00	3.00	16.0	64.0
1981		Epoxy	3G/8CHS/3G	1380	102	1.36	1520.00	135.00	1.12	1200.00	39.00	3.00	57.0	19.0
1981		Epoxy	1G/9CHS/1G	1400	109	1.29	1520.00	135.00	1.12	1200.00	39.00	3.00	82.0	7.0
1981		Epoxy	8G/9CHS/8G	1030	81	1.27	1520.00	135.00	1.12	1200.00	39.00	3.00	36.0	36.0
1981		Epoxy	1G/1CHM/1G	750	95	0.79	1330.00	192.00	0.69	1200.00	39.00	3.00	33.0	15.0
1981		Epoxy	2G/2CHM/2G	830	99	0.84	1330.00	192.00	0.69	1200.00	39.00	3.00	33.0	22.0
1981		Epoxy	3G/3CHM/3G	750	89	0.84	1330.00	192.00	0.69	1200.00	39.00	3.00	33.0	22.0
1981		Epoxy	6G/7CHM/6G	820	100	0.82	1330.00	192.00	0.69	1200.00	39.00	3.00	37.0	19.0
1981		Epoxy	8G/3CHM/8G	550	65	0.84	1330.00	192.00	0.69	1200.00	39.00	3.00	16.0	22.0
1981		Epoxy	9G/1CHM/9G	510	50	1.01	1330.00	192.00	0.69	1200.00	39.00	3.00	5.0	46.0
1981	[73]	Epoxy	Intralayer	265	20	1.30	1467.57	125.40	1.12	1322.88	47.89	2.84	90	16.1
1981		Epoxy	Intralayer	191	17.8	1.06	1467.57	125.40	1.12	1322.88	47.89	2.84	80	-5.4
1981		Epoxy	Intralayer	84.7	30.4	0.38	1051.41	185.69	0.54	1324.95	47.89	2.84	90	-29.0
1981		Epoxy	Intralayer	81.3	29.6	0.31	1051.41	185.69	0.54	1324.95	47.89	2.84	80	-42.1
1981		Epoxy	Intralayer	109	24.1	0.45	1051.41	185.69	0.54	1324.95	47.89	2.84	70	-15.9
1981		Epoxy	Intralayer	196	18.5	0.38	1472.39	125.40	1.12	1281.54	77.17	1.73	90	-66.1
1981		Epoxy	Intralayer	204	17.8	1.13	1472.39	125.40	1.12	1281.54	77.17	1.73	80	0.9
1981		Epoxy	Intralayer	205	16.8	1.01	1472.39	125.40	1.12	1281.54	77.17	1.73	70	-9.8

Table 8 — (Continued)

Year	Ref.	Matrix	Stacking sequence	Tensile strength [MPa]	Elastic modulus [GPa]	Strain at the failure [%]	S_L	E_L	ε_L	S_H	E_H	ε_H	Vol% LS [%]	Hybrid effect [%]
1981	[73]	Epoxy	Intralayer	103	26.8	0.37	1051.41	182.59	0.54	1281.54	77.17	1.73	90	-30.8
1981		Epoxy	Intralayer	105	26.9	0.38	1051.41	182.59	0.54	1281.54	77.17	1.73	80	-29.0
1981		Epoxy	Intralayer	110	25.9	0.43	1051.41	182.59	0.54	1281.54	77.17	1.73	70	-19.6
2007	[17]	Epoxy	1C/1G	3305	162.0	2.04	4214.00	242.00	1.74	2121.00	87.00	2.45	48.5	17.2
2007		Epoxy	1C/1B	2271	166.0	1.67	4214.00	242.00	1.74	2332.00	87.00	2.56	50	-4.0
2010	[74]	Polypropylene	2SRPP/1C/2SRPP	219	15.4	1.27	644.00	50.70	1.19	149.00	2.80	21.70	17.0	7.0
2010		Polypropylene	1C/2SRPP/1C	398	26.3	1.41	644.00	50.70	1.19	149.00	2.80	21.70	33.0	18.0
2010		Polypropylene	1SRPP/1C/1SRPP /1C/1SRPP	347	22.8	1.31	644.00	50.70	1.19	149.00	2.80	21.70	28.0	10.0
2011	[75]	Epoxy	3G/4C/3G	436	27.0	2.59	511.00	39	1.36	322.00	12.5	4.25	47.0	90.4
2011		Epoxy	2C/6G/2C	421	27.5	1.86	511.00	39	1.36	322.00	12.5	4.25	47.0	36.8
2011	[76]	Epoxy	1C/1B	2409	142.0	1.74	4067.00	239.80	1.74	2145.00	81.50	2.76	41.57	0.0
2011		Epoxy	1C/2B	2186	125.0	1.84	4067.00	239.80	1.74	2145.00	81.50	2.76	26.24	5.7
2013	[77]	Phenolic	1G/8F/1G		32.3	0.99		29.04	0.85		51.22	1.41	86.0	16.5
2013		Phenolic	1G/2F/1G/2F/1G/ 2F/1G		36.4	1.12		29.04	0.85		51.22	1.41	69.0	31.8
2013		Phenolic	1G/1F/1G/1F/2G/ 1F/1G/1F/1G		40.9	1.25		29.04	0.85		51.22	1.41	50.0	47.1
2013		Phenolic	3G/1F/2G/1F/3G		45.0	1.37		29.04	0.85		51.22	1.41	27.0	61.2
2013	[1]	Epoxy	2G/1C/2G	967	44.0	2.20	1962.00	101.70	1.50	1548.00	38.70	3.40	4.9	18.4

Table 8 — (Continued)

Year	Ref.	Matrix	Stacking sequence	Tensile strength [MPa]	Elastic modulus [GPa]	Strain at the failure [%]	S_L	E_L	ε_L	S_H	E_H	ε_H	Vol% LS [%]	Hybrid effect [%]
2013	[1]	Epoxy	2G/2C/2G	954	47.0	2.06	1962.00	101.70	1.50	1548.00	38.70	3.40	9.4	10.9
2013		Epoxy	2G/3C/2G	965	49.0	1.92	1962.00	101.70	1.50	1548.00	38.70	3.40	13.4	3.3
2013		Epoxy	2G/4C/2G	985	51.0	1.93	1962.00	101.70	1.50	1548.00	38.70	3.40	17.2	3.9
2014	[78]	Epoxy	1B/1C	2482	145.0	1.74	4067.00	239.80	1.74	2077.00	80.20	2.68	41.6	0.0
2014		Epoxy	2B/1C	2213	124.0	1.84	4067.00	239.80	1.74	2077.00	80.20	2.68	26.2	5.7
2014	[79]	Epoxy	4C/1B/5C	630	60.0	1.07	687.00	65.00	1.06	402.00	18.00	2.20	92.2	0.8
2014		Epoxy	4C/2B/4C	602	55.0	1.10	687.00	65.00	1.06	402.00	18.00	2.20	84.0	3.1
2014		Epoxy	3C/3B/4C	558	50.0	1.10	687.00	65.00	1.06	402.00	18.00	2.20	75.4	3.6
2014		Epoxy	3C/4B/3C	536	45.0	1.14	687.00	65.00	1.06	402.00	18.00	2.20	66.4	7.3
2014		Epoxy	2C/5B/3C	502	40.0	1.20	687.00	65.00	1.06	402.00	18.00	2.20	56.8	13.0
2014		Epoxy	2B/6C/2B	571	49.5	1.15	687.00	65.00	1.06	402.00	18.00	2.20	66.4	8.3
2014		Epoxy	2C/2B/2C/2B/2C	556	47.5	1.17	687.00	65.00	1.06	402.00	18.00	2.20	66.4	10.2
2016	[80]	Epoxy	1C/1G/1C/1G	1034	57.0	2.01	4400.00	235.00	1.70	1838.00	73.10	4.51	56.0	18.2
2016	[28]	Epoxy	1G/1C/1G			2.17	1962.00	101.00	1.50	2138.00	45.70	4.51	8.6	16.6
2016		Epoxy	1G/2C/1G			1.96	1962.00	101.00	1.50	2138.00	45.70	4.51	15.8	5.7
2016		Epoxy	1G/3C/1G			1.84	1962.00	101.00	1.50	2138.00	45.70	4.51	21.9	-1.0
2016		Epoxy	2G/4C/2G			1.88	1962.00	101.00	1.50	2138.00	45.70	4.51	15.8	1.0

Notes: CHS – high-tensile carbon; SRPP – self-reinforced polypropylene; F – flax.

Table 9 — Analytical model input data.

Material combination	Series ID	G_{IIC} [kN/m]	E_H [GPa]	E_L [GPa]	S_H [MPa]	S_L [MPa]	ε_H [%]	ε_L [%]	K_t	W [mm]	L [mm]	m_H	t_H [mm]	t_L [mm]
C/B	1C/1B/1C	1.90	102.5	231.3	2244.2	2289.9	2.46	0.99	0.97	15	150	29.3	0.0785	0.2230
	1B/1C/1B	1.90	102.5	231.3	2244.2	2960.6	2.46	1.28	0.97	15	150	29.3	0.1570	0.1115
CHM/B	1CHM/1B/1CHM	1.90	102.5	624.1	2244.2	1497.8	2.46	0.24	0.97	15	150	29.3	0.0785	0.1900
	1B/1CHM/1B	1.90	102.5	624.1	2244.2	2246.8	2.46	0.36	0.97	15	150	29.3	0.1570	0.0950
CHM/C	1CHM/1C/1CHM	1.25	231.3	624.1	2565.9	1684.8	1.09	0.27	0.97	15	150	29.3	0.1115	0.1900
	1C/1CHM/1C	1.25	231.3	624.1	2565.9	2434.0	1.09	0.39	0.97	15	150	29.3	0.223	0.0950
C/G	1C/1G/1C	1.90	81.6	231.3	1671.2	2405.0	2.31	1.04	0.97	15	150	29.3	0.0770	0.2230
	1G/3C/1G	1.90	81.6	231.3	1671.2	2521.2	2.31	1.09	0.97	15	150	29.3	0.1540	0.3345
	1G/1C/1G/1C/1G	1.90	81.6	231.3	1671.2	2752.5	2.31	1.19	0.97	15	150	29.3	0.2310	0.2230
	1G/1C/1G	1.90	81.6	231.3	1671.2	2937.5	2.31	1.27	0.97	15	150	29.3	0.1540	0.1115
	2G/1C/2G	1.90	81.6	231.3	1671.2	2706.2	2.31	1.17	0.97	15	150	29.3	0.3080	0.1115
CHM/G	1CHM/1G/1CHM	1.46	81.6	624.1	1671.2	1560.3	2.31	0.25	0.97	15	150	29.3	0.0770	0.1900
	1G/3CHM/1G	1.46	81.6	624.1	1671.2	1435.4	2.31	0.23	0.97	15	150	29.3	0.1540	0.2850
	1G/1CHM/1G/1CHM/1G	1.46	81.6	624.1	1671.2	2184.4	2.31	0.35	0.97	15	150	29.3	0.2310	0.1900
	1G/1CHM/1G	1.46	81.6	624.1	1671.2	1872.0	2.31	0.30	0.97	15	150	29.3	0.154	0.0950
	2G/1CHM/2G	1.46	81.6	624.1	1671.2	2059.5	2.31	0.33	0.97	15	150	29.3	0.3080	0.0950

Notes: t_H – half thickness of the high strain material; t_L – half thickness of the low strain material.

List of Figures

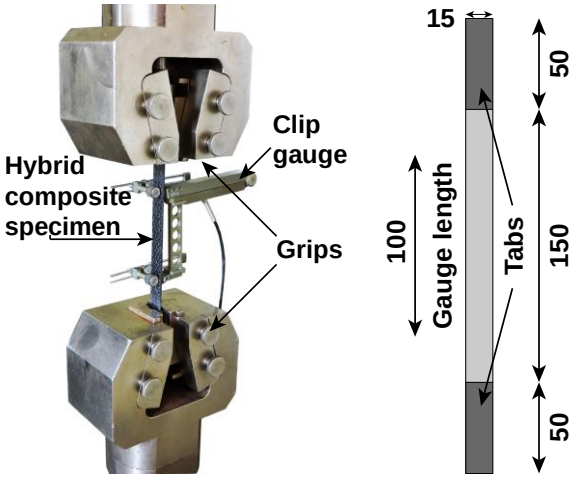

(a) (b)

Figure 1 — Tensile test: (a) illustration of the test and (b) geometry of specimen (dimensions in mm).

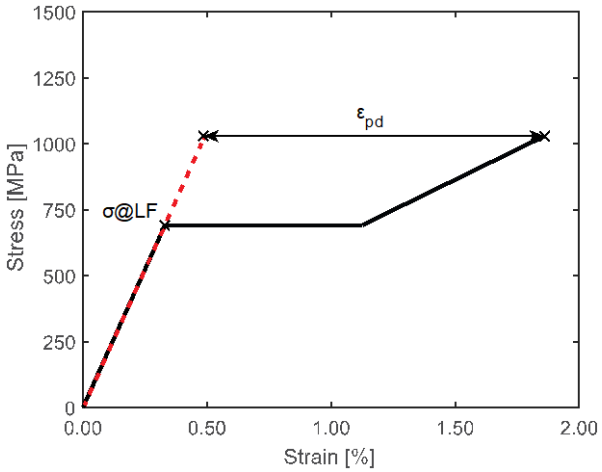

Figure 2 — Illustration of nonlinear pseudo-ductile behaviour and definition of 'yield' stress and pseudo-ductile strain (adapted from [2]).

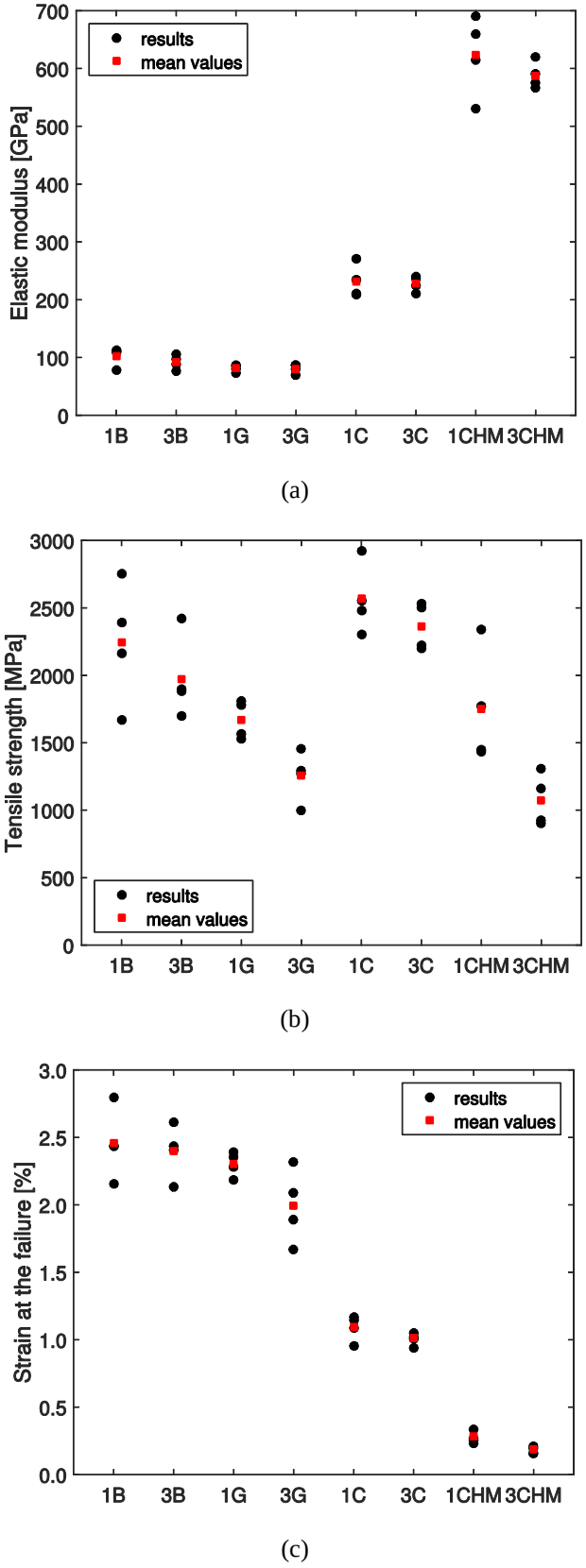

Figure 3 — Scatter diagrams and mean values of the non-hybrid composites tensile properties: (a) elastic modulus; (b) tensile strength and (c) strain at the failure.

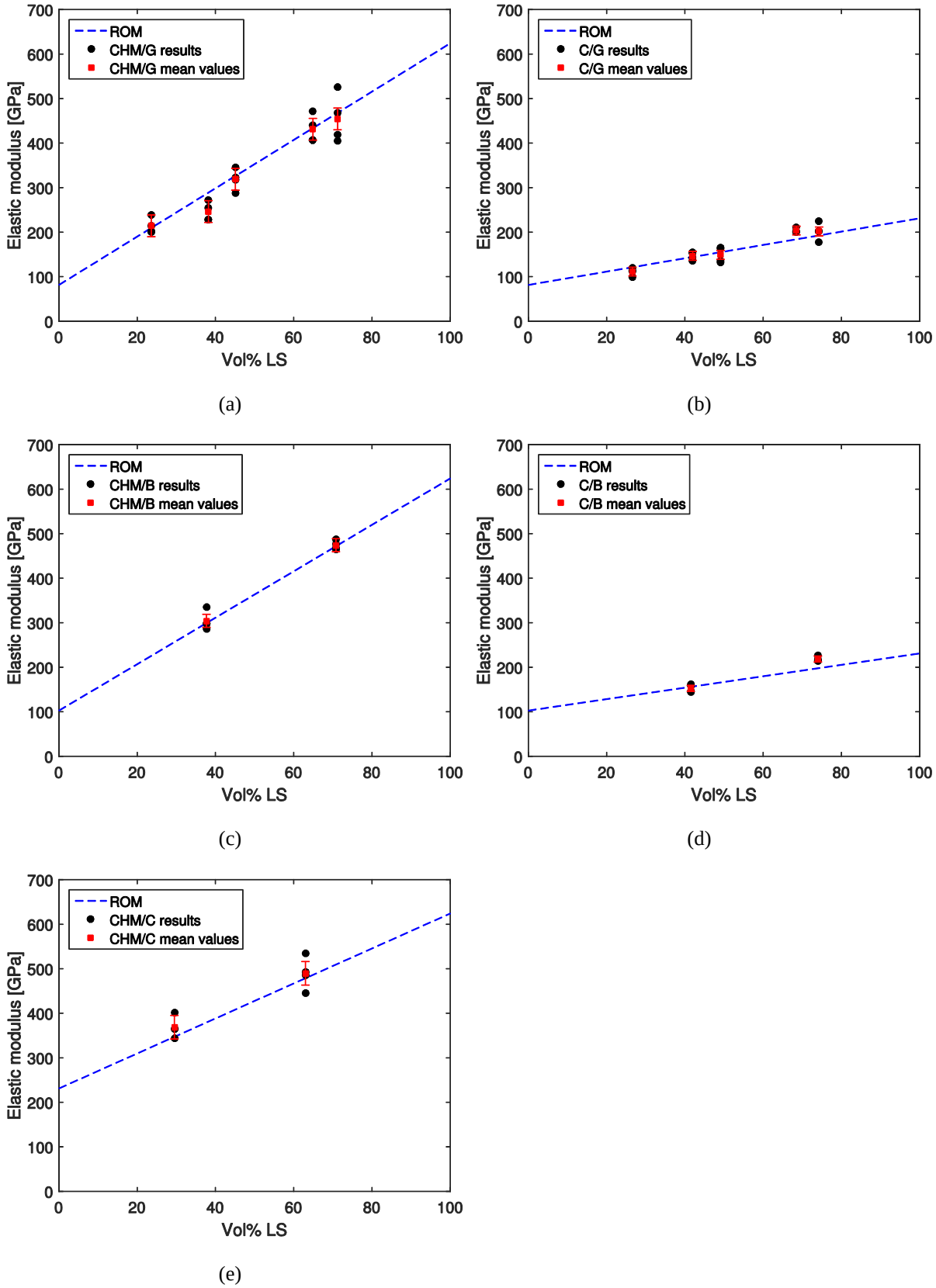

Figure 4 — Elastic modulus as function of the LS fibres vol% of the: HM carbon/glass; (b) ST carbon/glass; (c) HM carbon/basalt; (d) ST carbon/basalt and (e) HM carbon/ST carbon.

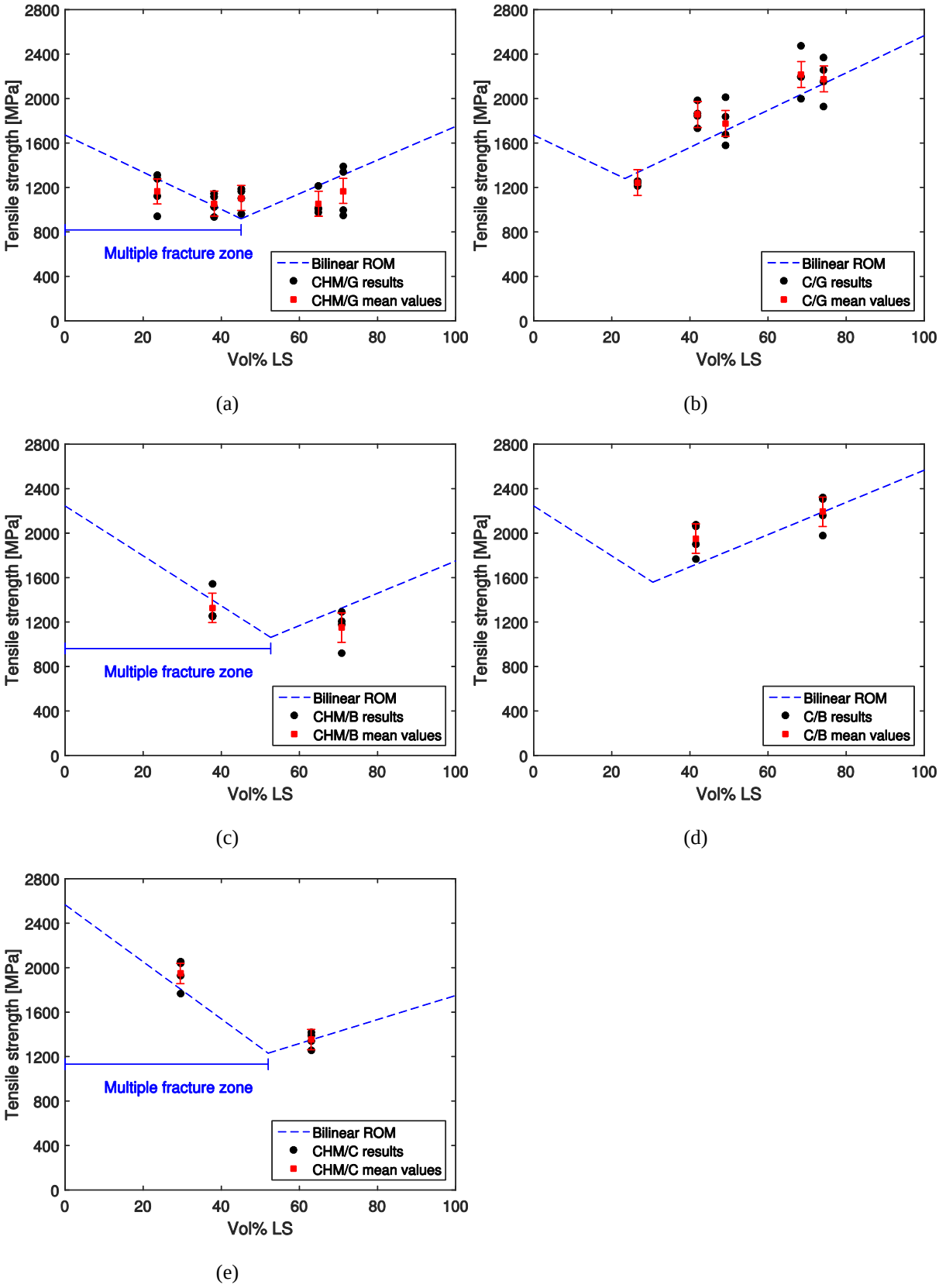

Figure 5 — Tensile strength as function of the LS fibres vol% of the: (a) HM carbon/glass; (b) ST carbon/glass; (c) HM carbon/basalt; (d) ST carbon/basalt and (e) HM carbon/ST carbon composites.

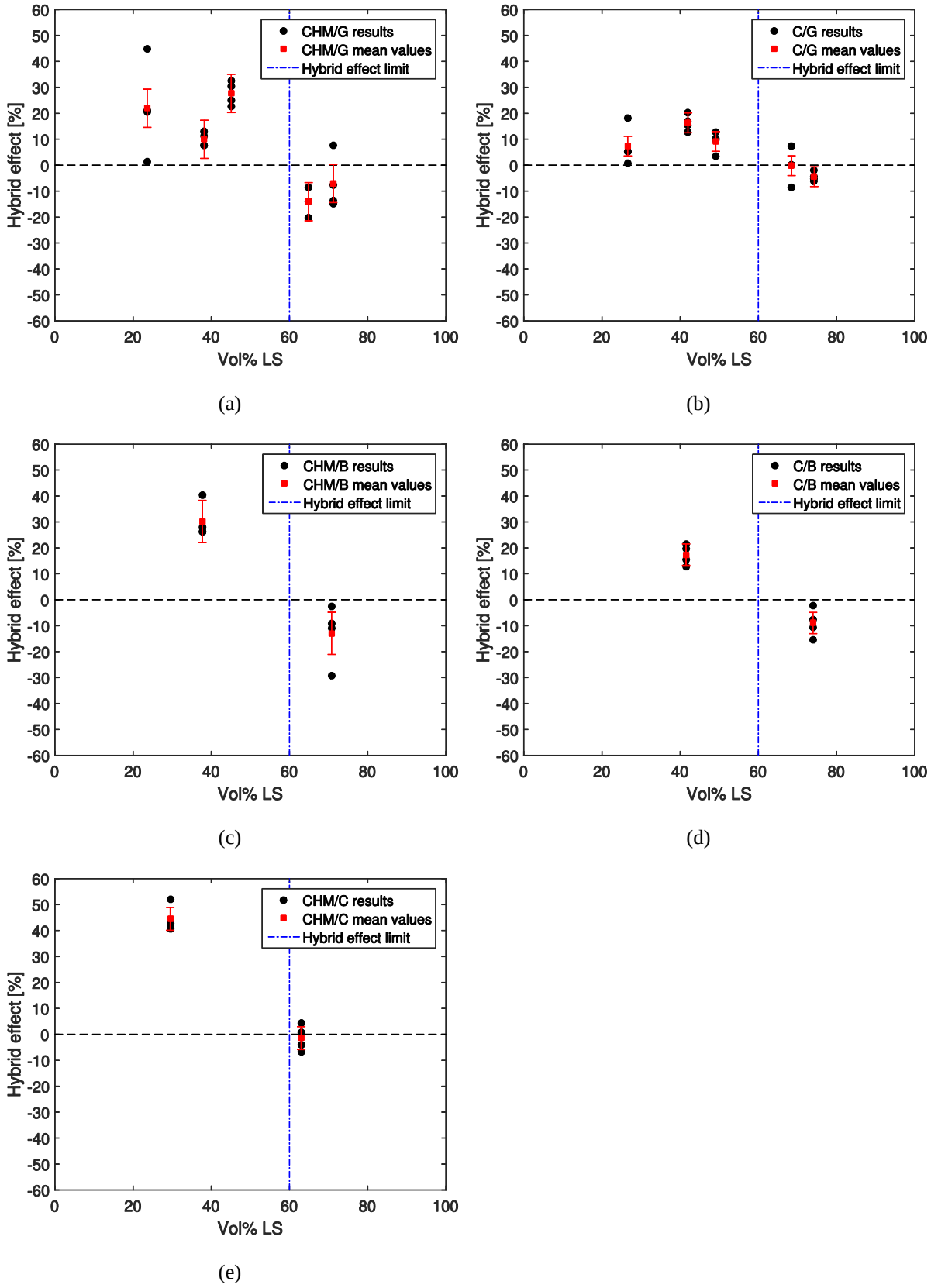

Figure 6 — Hybrid effect in function of the LS fibres volume fraction fo the: (a) HM carbon/glass; (b) ST carbon/glass; (c) HM carbon/basalt; (d) ST carbon/basalt and (e) HM carbon/ST carbon composites.

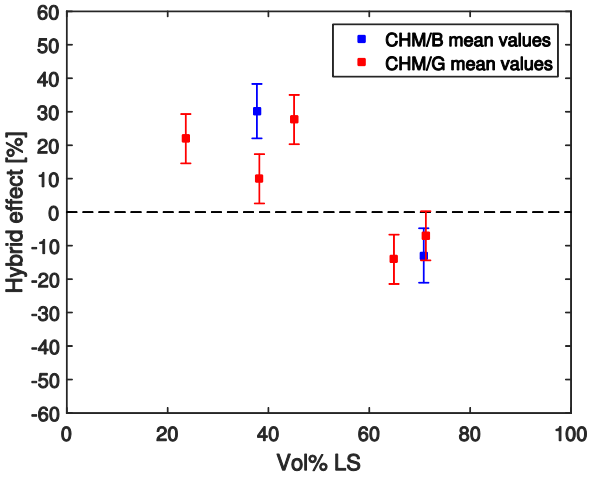

(a)

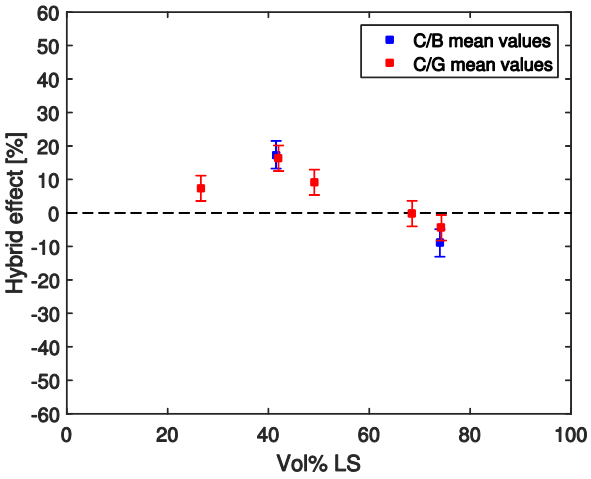

(b)

Figure 7 — Differences in hybrid effect caused by replacing glass with basalt: (a) HM carbon series and (b) ST carbon series.

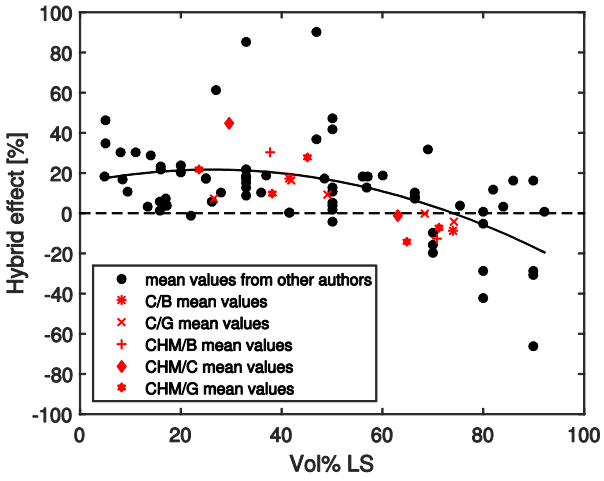

(a)

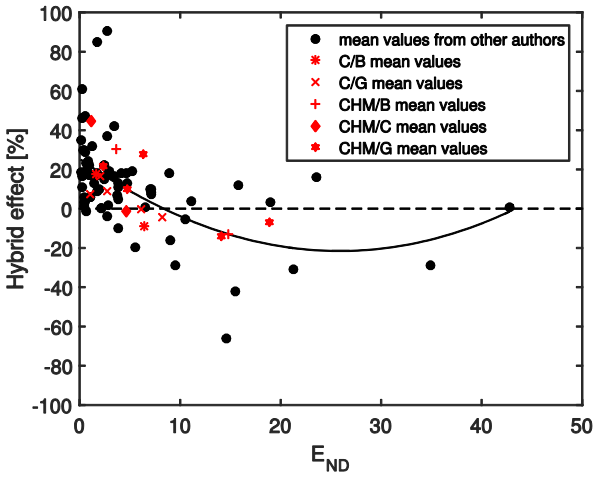

(b)

Figure 8 — Scatter diagrams of hybrid effect mean results obtained in this work compared against mean results from other authors: (a) as function of LS fibres vol% and (b) as function of E_{ND}.

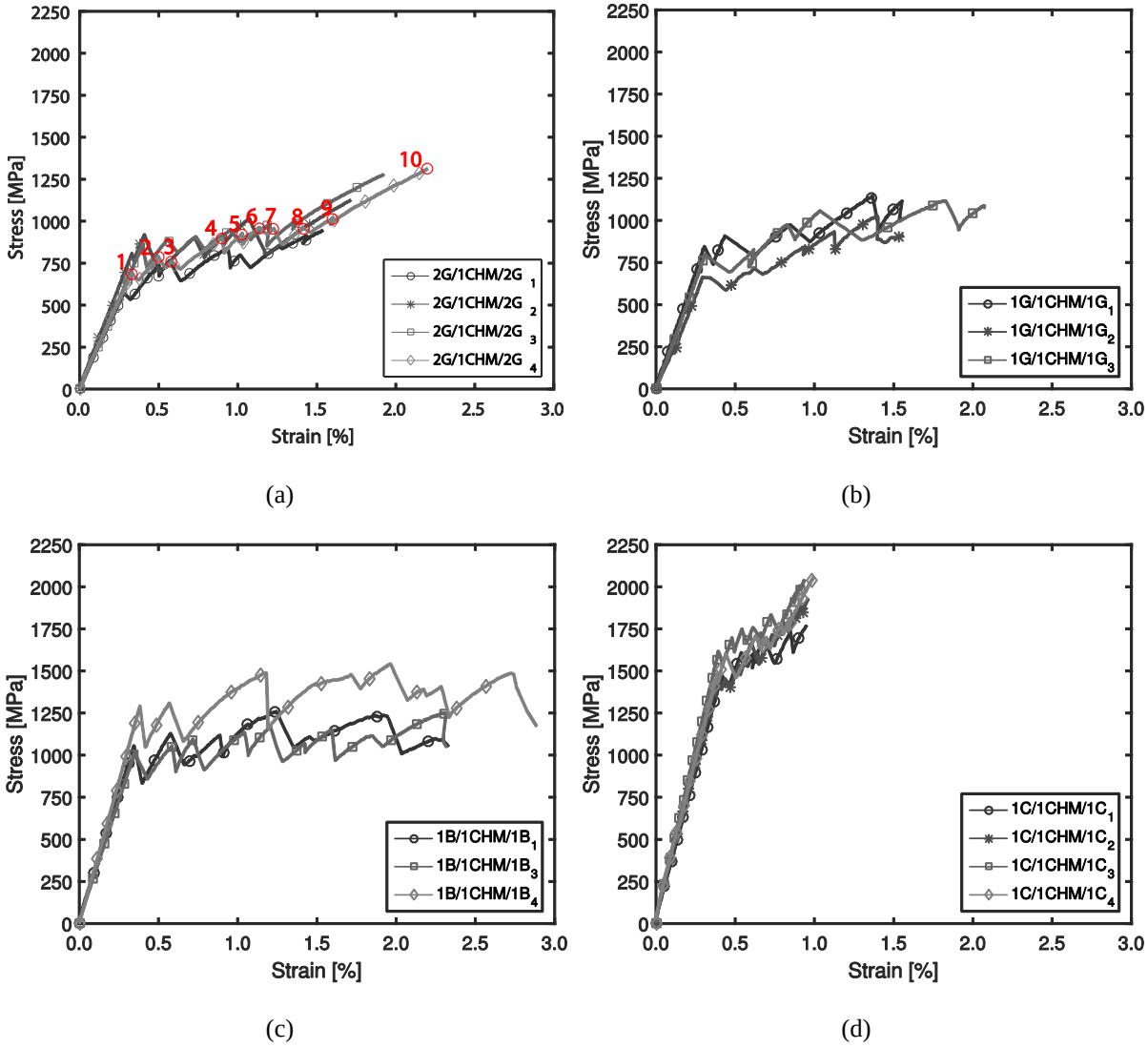

Figure 9 — Pseudo-ductile tensile responses: (a) 2G/1CHM/2G; (b) 1G/1CHM/1G; (c) 1B/1CHM/1B and (d) 1C/1CHM/1C series.

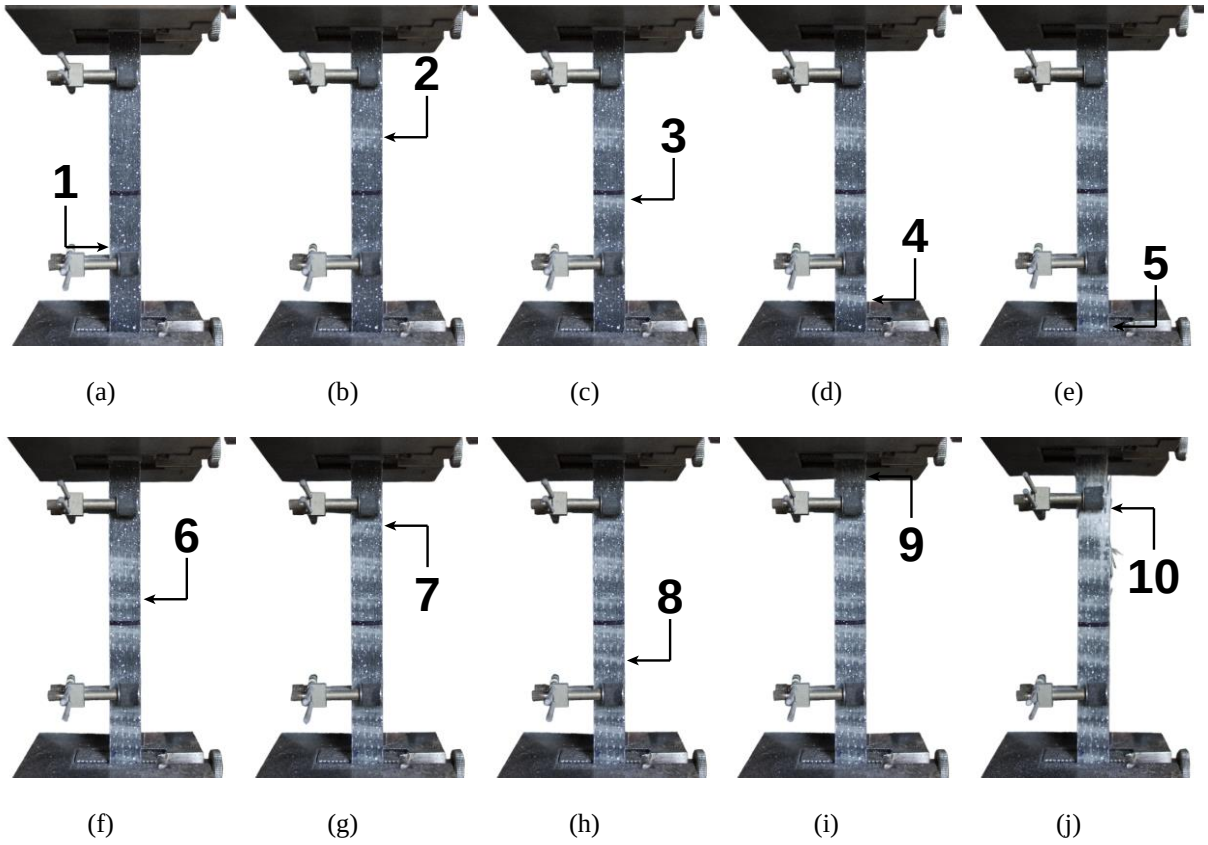

Figure 10 — Example of localised delamination around multiple cracked HM carbon-layer that occurred until the final rupture in 2G/1CHM/2G 4th specimen: (a) 1st peak; (b) 2nd peak; (c) 3rd peak; (d) 4th peak; (e) 5th peak; (f) 6th peak; (g) 7th peak; (h) 8th peak; (i) 9th peak and (j) final rupture.

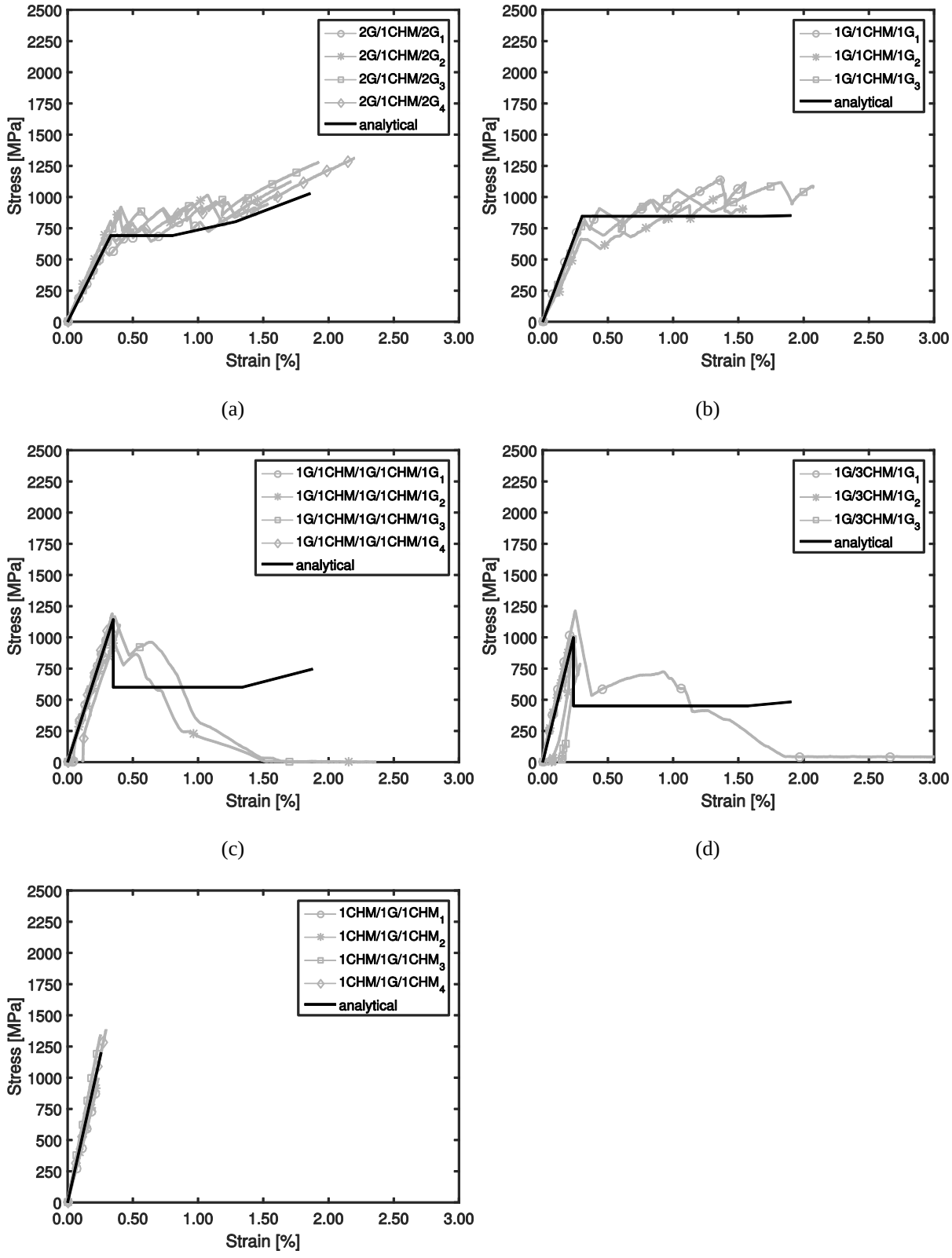

Figure 11 — Stress–strain curves of CHM/G combinations: experimental versus predicted values.

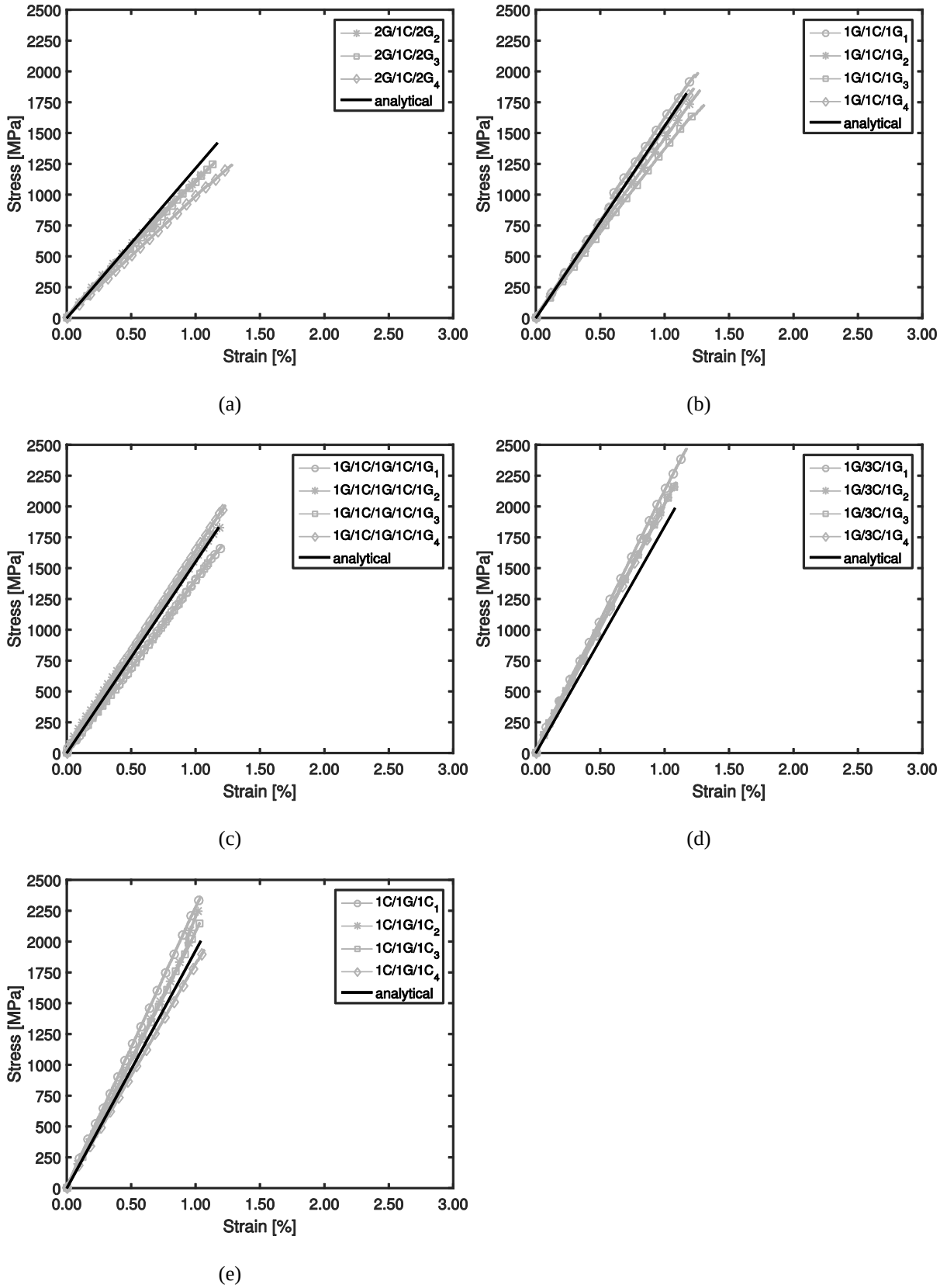

Figure 12 — Stress–strain curves of C/G combinations: experimental *versus* predicted values.

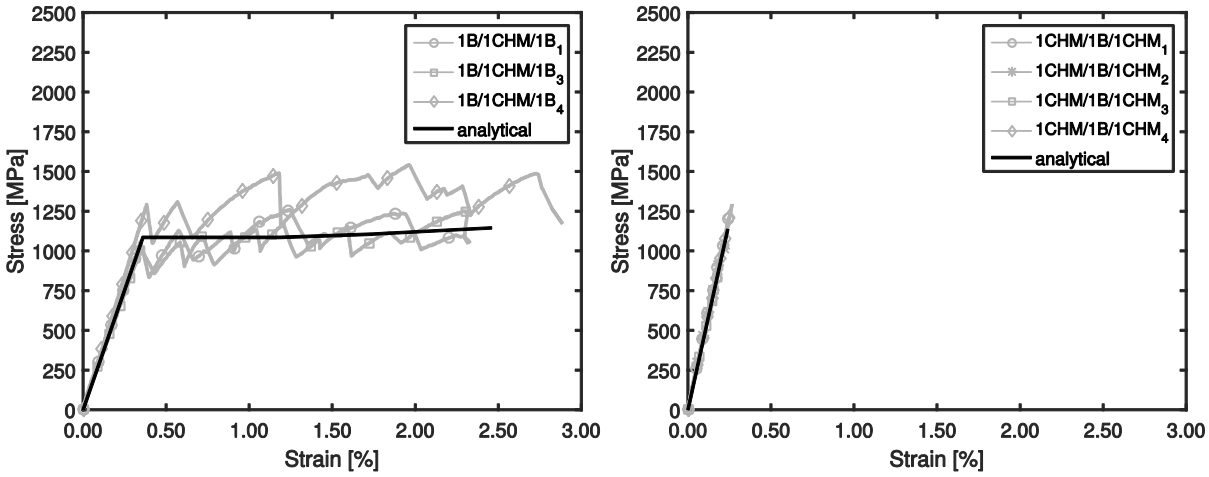

(a) (b)

Figure 13 — Stress–strain curves of CHM/B combinations: experimental *versus* predicted values.

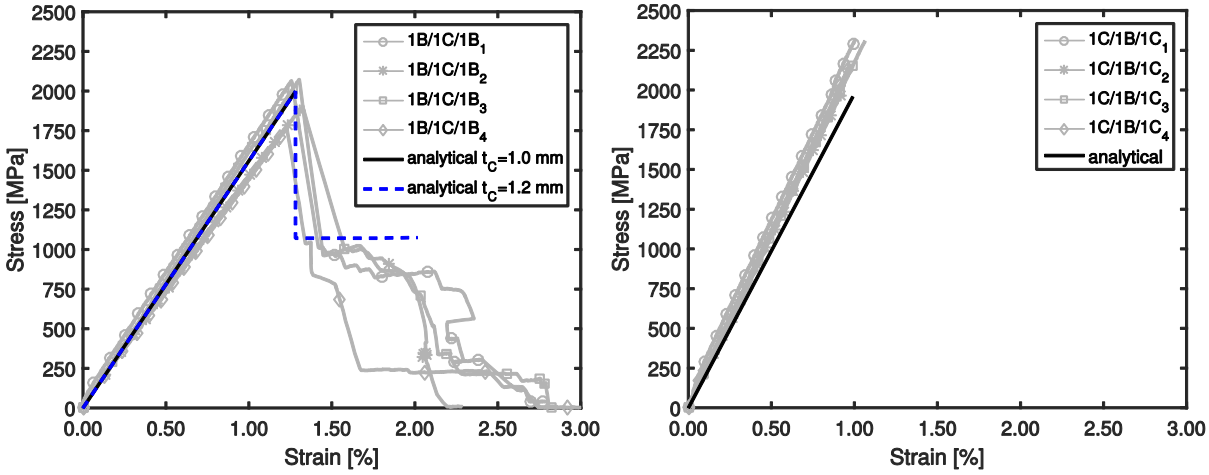

(a) (b)

Figure 14 — Stress–strain curves of C/B combinations: experimental *versus* predicted values.

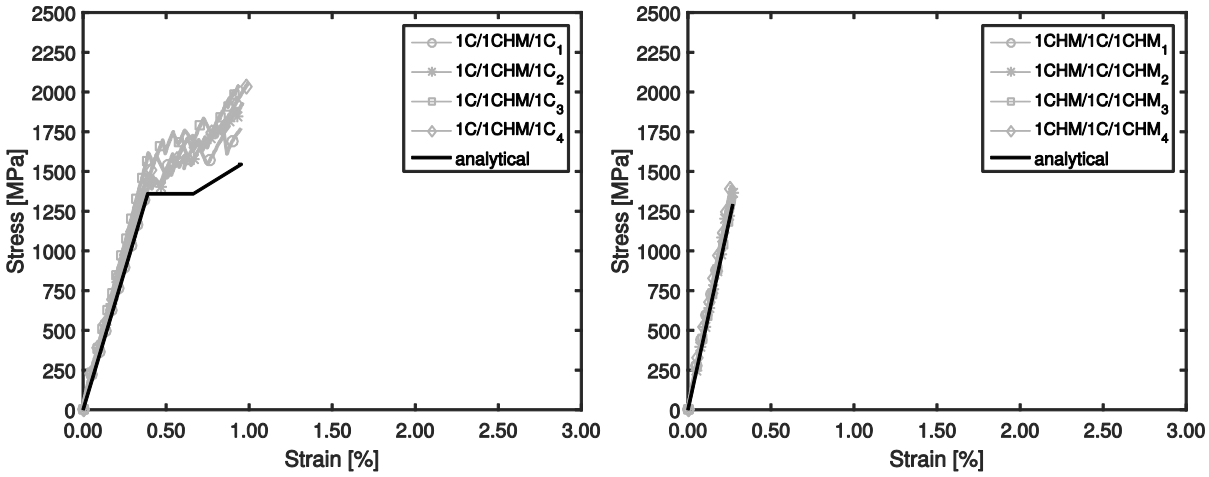

(a) (b)

Figure 15 — Stress–strain curves of CHM/C combinations: experimental *versus* predicted values.